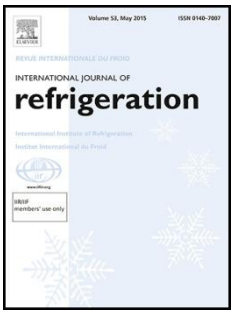

Title: Modified homogeneous relaxation model for the r744 trans-critical flow in a two-phase ejector

Author: Michal Haida, Jacek Smolka, Armin Hafner, Michal Palacz, Krzysztof Banasiak, Andrzej J. Nowak

PII: S0140-7007(17)30394-8
DOI: https://doi.org/doi:10.1016/j.ijrefrig.2017.10.010
Reference: JIJR 3778

To appear in: *International Journal of Refrigeration*

Received date: 27-6-2017
Revised date: 27-9-2017
Accepted date: 8-10-2017

Please cite this article as: Michal Haida, Jacek Smolka, Armin Hafner, Michal Palacz, Krzysztof Banasiak, Andrzej J. Nowak, Modified homogeneous relaxation model for the r744 trans-critical flow in a two-phase ejector, *International Journal of Refrigeration* (2017), https://doi.org/doi:10.1016/j.ijrefrig.2017.10.010.

Modified homogeneous relaxation model for the R744 trans-critical flow in a two-phase ejector

Michal Haida[a*], Jacek Smolka[a], Armin Hafner[b], Michal Palacz[a], Krzysztof Banasiak[c], Andrzej J. Nowak[a]

[a] Institute of Thermal Technology, Silesian University of Technology, Konarskiego 22, Gliwice 44-100, Poland
[b] NTNU Department of Energy and Process Engineering, Kolbjørn Hejes vei 1d, 7465 Trondheim, Norway
[c] SINTEF Energy Research, Kolbjørn Hejes vei 1d, 7465 Trondheim, Norway

Highlights

- The modified homogeneous relaxation model of the R744 two-phase ejector was proposed.
- The application range of the proposed model is for a motive nozzle pressure above 59 bar.
- The proposed model improved the motive nozzle mass flow rate accuracy when compared to the homogeneous equilibrium model.

Abstract

The proposed modified homogeneous relaxation model (HRM) applied to the numerical model of a CO_2 two-phase ejector was numerically investigated and developed based on the optimisation of the relaxation time (RT) correlation. The optimisation procedure was performed using a genetic algorithm. The study of the RT definition on model accuracy was carried out using literature correlations, constant relaxation time, and by comparing the developed modified HRM with experimental results. The modified HRM showed the higher accuracy of the motive nozzle mass flow rate (MFR) than that of the other available numerical models for the subcritical operating regimes and similar high accuracy as the homogeneous equilibrium model (HEM) for the trans-critical operating regimes. The application range of the modified HRM was defined for the motive nozzle pressure above 59 bar to predict the

* Corresponding author. Tel: +48 32 2371661
E-mail address: Michal.Haida@polsl.pl (Michal Haida)

motive nozzle MFR with the relative error below 15%. For the motive nozzle pressure level below 59 bar, the modified HRM improved the accuracy of the motive MFR prediction by 5% to 10% compared to the HEM formulation.

Keywords: R744, ejector, two-phase flow, relaxation model, relaxation time, refrigeration system

Nomenclature

Roman Letter

dP	Pressure lift	bar
E	Total enthalpy	kJ kg^{-1}
h	Specific enthalpy	kJ kg^{-1}
k	Effective thermal conductivity	W m^{-1} K^{-1}
s	Specific entropy	kJ kg^{-1} K^{-1}
$\dot{m}$	Mass flow rate	kg s^{-1}
p	Pressure	bar
t	Time	s
T	Temperature	K
$\boldsymbol{u}$	Velocity vector	m s^{-1}
x	Local vapour quality	

Greek Letters

α	Void fraction	
φ	Non dimensional pressure difference	
δ	Relative error	%
θ	Relaxation time	s
Φ	Mass entrainment ratio	
Π	Pressure ratio	
ρ	Density	kg m^{-3}
$\boldsymbol{\tau}$	Stress tensor	N m^{-2}
Γ	Vapour generation rate	kg m^{-3} s^{-1}

Subscripts

crit	Critical conditions
eq	Equilibrium state
exp	Experimental result
motive	Motive parameter
ml	Metastable conditions
num	Numerical result
opt	Optimal value
sat	Saturation line
suction	Suction parameter
sv	Saturated vapour

Abbreviations

EERC	Ejector expansion refrigeration cycle
GA	Genetic algorithm
HEM	Homogenous equilibrium model
HRM	Homogenous relaxation model
MFR	Mass flow rate
OC	Operating condition
OF	Objective function
RT	Relaxation time

Other symbols

$\bar{n}$	Reynolds averaged
$\tilde{n}$	Favre averaged

1 Introduction

Due to the restrictive legal regulations for environmental protection in refrigeration, common synthetic refrigerants are replaced by environmentally friendly natural refrigerants, such as carbon dioxide (denoted as R744). R744 is classified as a non-toxic and a non-flammable fluid with the low global warming potential index GWP of 1, and ozone depletion potential index of 0. Lorentzen was one of the first researchers who proposed and then patented a trans-critical carbon dioxide system for automotive air conditioning. This led to the design and manufacturing of comparative refrigeration systems with CO_2 as the main working fluid when

compared to the cooling system with the classical synthetic refrigerant, i.e. R134a (Lorentzen, 1990). Currently, the R744 refrigeration systems are mostly introduced in cold climates as the result of the relatively low efficiency at high surrounding temperatures. One of the solutions to improve the energy performance of the CO_2 trans-critical refrigeration cycle is the implementation of the two-phase ejector as the main expansion device in the cycle.

The replacement of the expansion valve with the ejector in the CO_2 trans-critical vapour compression cycle improves energy performance as reported in theoretical and experimental investigations (Sumeru et al., 2012). Li and Groll (2005) analysed the CO_2 ejector expansion refrigeration cycle (EERC) based on the modified non-dimensional ejector solver proposed by Kornhauser (1990). The authors stated that the coefficient of performance (COP) improvement of the EERC was more than 16% at the typical air conditioning operating conditions. The energy performance improvement of the R744 ejector expansion trans-critical cycle up to 18.6% was indicated by Deng et al. (2007). However, the authors concluded that the experimental investigation of the R744 refrigeration cycle with a well-designed ejector is required. Elbel and Hrnjak (2008) presented the experimental investigation of the trans-critical R744 cycle with a prototype ejector. The experimental results confirmed the energy performance improvement of the EERC up to 7% and the influence of the ejector geometry on the COP value. The two-phase ejector with designed geometry, based on the delayed equilibrium model, improved the energy performance of the R744 refrigeration system up to 8% (Banasiak et al., 2012).

Hafner et al. (2014) presented the design concept of the R744 multi-ejector system with non-continuously controllable ejectors for a supermarket application. The steady-state simulation for the ejector constant efficiency of 20% showed COP improvement between 10% at 15 °C and 20% at 45 °C ambient temperature compared to the reference booster system. Transient simulations were performed based on the annual variable ambient temperature and annual variable load profiles for heating and cooling modes for three different climate regions. The COP for cooling mode increased between 20% and 30% during the winter and 17% in the Mediterranean region, 16% in Middle Europe, and 5% in Northern Europe during the summer. Haida et al. (2016) presented the experimental investigation of the R744 multi-ejector refrigeration system based on energy and exergy analysis. The author stated that the COP and the exergy efficiency of the multi-ejector system increased up to 8% and 13.7% compared to the reference parallel-compression system at the typical supermarket operating conditions.

The dynamic simulations and the experimental investigation of the R744 multi-ejector system indicated high potential of the two-phase ejector implementation in the refrigeration system. The ejectors designed for such systems should offer high efficiency for the considered operating conditions. Various complex numerical models were formulated to analyse and design the CO_2 ejectors (Elbel and Lawrence, 2016). The computational fluid dynamics (CFD) model of the ejector required information about the flow turbulence to properly predict the mass flow rates of both streams. Mazzelli et al. (2015) investigated the supersonic ejector performance prediction of different turbulence models based on the experimental and numerical analyses. The authors stated that each turbulence model predicted the motive and suction nozzle mass flow rates (MFR) with small differences compared to the experimental results. The *k-ω* SST model obtained the best accuracy compared to the *ε*-based models. The numerical investigation of the different turbulence models implemented with the numerical steam ejector model by Besagni and Inzoli (2017) confirmed that the *k-ω* SST model reached the best agreement with the experimental data concerning global and local flow quantities.

The homogeneous fluid flow assumption in the numerical model allows for the prediction of the two-phase flow behaviour inside the ejector. Lucas et al. (2014) used HEM to simulate the R744 two-phase flow inside the ejector. The numerical results showed the discrepancy of the CFD model motive nozzle mass flux within 10% and the accuracy of the pressure recovery was 10% without the suction flow entrainment and 20% with the suction flow. Smolka et al. (2013) performed three-dimensional modelling of the single- and two-phase flow of a real fluid based on the enthalpy-based energy equation, in which the specific enthalpy was an independent variable. The computational model was tested and validated for the single-phase R141b ejector, and for the two-phase R744 ejector. This approach was successfully followed in the work of Giacomelli et al. (2016). The foregoing HEM was used to design and manufacture the multi-ejector expansion pack with four different ejectors with a binary profile for the R744 parallel-compression refrigeration system (Palacz et al., 2015), which was experimentally investigated by Banasiak et al. (2015).

Palacz et al. (2017b) used genetic and evolutionary algorithms to optimise the ejector shape of the R744 two-phase ejector based on the HEM at the operating conditions typical for supermarket application. The optimisation procedure was performed on four ejectors with different capacity to maximise each ejector's efficiency. The authors indicated ejector efficiency improvement up to 6% compared to the designed ejector for a multi-ejector R744 supermarket refrigeration system. Apart from the numerical investigation and the shape

optimisation of the two-phase ejector, HEM was used to analyse the two most common types of the diesel injector nozzles (Salvador et al., 2015).

Palacz et al. (2015) analysed the HEM accuracy, which was applied to three-dimensional CFD-based simulations of R744 expansion inside a two-phase ejector. The computational results of the motive nozzle MFR were compared to the measured MFR for a wide range of operating conditions. The analysis showed the acceptable application of the HEM approach for the operating regimes near or above the critical point. Unfortunately, the inaccuracy of the model increased with decreasing motive nozzle temperature and decreasing distance to the saturation line. According to Palacz et al. (2015), more complex mathematical models such as the homogenous relaxation model (HRM) should be used to improve the optimisation tool for a wider range of the operating conditions.

HRM was proposed by Bilicki and Kestin (1990) as a linearised expansion. The authors described the difference in HEM and HRM approaches with special attention to a study of dispersion, characteristics, choking and shock waves. The relation of the empirical correlation of the relaxation time (RT) and the quality of the flashing fluid was described in Bilicki and Kestin (1990). Downar-Zapolski et al. (1996) presented the comparison of the results obtained on the basis of the HRM and HEM solutions and available experimental data. The validation procedure was performed for one-dimensional flashing water flow to predict the critical MFRs and the pressure distributions. HRM predicted with good accuracy both the pressure distributions and the critical MFRs, while HEM underestimated the critical MFRs by over 20% for a small value of inlet sub-cooling (Downar-Zapolski et al., 1996).

The investigation of HRM for the CO_2 supersonic two-phase flow through the ejector motive nozzle was presented in the work of Angielczyk et al. (2010). The numerical results were validated for three different converging-diverging nozzle diameters with the experimental results taken from Nakagawa et al. (2009). In addition, a new correlation for the CO_2 relaxation time was proposed. The authors concluded that the additional information such as temperature profiles, quality profiles and critical flow rate would be required to calibrate the numerical model and define a suitable correlation for the relaxation time.

Brown et al. (2013) developed and validated HRM for the full bore rupture of the dense phase CO_2 pipelines discharge behaviour simulations. The authors presented the impact of the various constant relaxation times together with the calculated relaxation time based on the definition given in the study of Angielczyk et al. (2010). According to Brown et al. (2013),

the numerical model predicted the discharge behaviour with reasonable accuracy in comparison to the limited real data. Omission of the delayed phase transition underestimated the discharge rate of CO_2 in the pipelines.

Colarossi et al. (2012) applied HRM for the R744 condensing two-phase ejector simulations based on the CFD open-source OpenFOAM model proposed by Schmidt et al. (2010). The CFD model was built based on the Eulerian pseudo-fluid approach. Surprisingly, the validation procedure of the pressure distribution of the ejector indicated high inaccuracy of the model in most cases, especially for a refrigeration system with the internal heat exchanger. According to Colarossi et al. (2012), the assumed motive nozzle inlet boundary conditions and the turbulence model strongly influenced the pressure prediction of the CFD results. Similar work was presented in the study of Palacz et al. (2017a) where the accuracy of HEM and HRM were compared for the R744 two-phase ejector at the operating conditions for supermarket applications. The relaxation time was defined based on the correlation presented by Angielczyk et al. (2010). The calculations of both models used the computational tool called *ejectorPL*; the results of the motive nozzle MFR and the entrainment ratio were compared based on the experimental results (Palacz et al., 2015). The authors stated that the HRM results obtained an accuracy improvement up to 5% compared to the HEM results, which was possibly caused by the relaxation time formulation.

The aim of this paper is to improve HRM applied in the CFD model of the R744 two-phase ejector and investigate the influence of the RT definition on the R744 two-phase flow behaviour. The study of the RT definition on model accuracy was performed using the literature correlations, constant values of the RT, and the modified RT. The correlation of RT was the result of the genetic algorithm optimisation procedure integrated with the *ejectorPL* computational tool. The constant coefficients that describe the RT correlation were parametrised to define the limitation of the objective function in the HRM optimisation procedure. The modified RT correlation was implemented to the modified HRM approach in order to extend the application range of the proposed model. The numerical results were validated with the experimental results carried out at the SINTEF Energy Research laboratory in Trondheim, Norway at typical supermarket refrigeration operating conditions.

2 Methodology

The modification of HRM required information about the mathematical formulation of the R744 two-phase ejector numerical model. The CFD model approach together with the

detailed description of HRM and the main parameters described in the two-phase ejector performance are presented in the following section.

2.1 HRM model approach

The numerical model of the two-phase flow inside the ejector was formulated based on the governing equations of mass, momentum and enthalpy conservation at the steady-state listed below (Smolka et al., 2013):

$$\nabla \cdot (\bar{\rho}\tilde{\boldsymbol{u}}) = 0 \tag{1}$$

$$\nabla \cdot (\bar{\rho}\tilde{\boldsymbol{u}}\tilde{\boldsymbol{u}}) = -\nabla \bar{p} + \nabla \cdot (\tilde{\boldsymbol{\tau}} + \boldsymbol{\tau}_T) \tag{2}$$

$$\nabla \cdot \left(\bar{\rho}\tilde{\boldsymbol{u}}\tilde{E}\right) = \nabla \cdot \left(k\nabla \tilde{T} + \tilde{\boldsymbol{\tau}} \cdot \tilde{\boldsymbol{u}}\right) \tag{3}$$

where the symbols $\bar{(\,)}$ and $\tilde{(\,)}$ denote the Reynolds- and Favre-averaged quantities, respectively. In addition, ρ is the fluid density, $\boldsymbol{u}$ is the velocity vector, p is the fluid pressure, $\boldsymbol{\tau}$ is the stress tensor, E is the total enthalpy, k is the effective thermal conductivity and T is the fluid temperature. The additional vapour mass balance equation is defined as the total derivative of the quality equal to the vapour generation rate divided by the total density.

$$\frac{D\tilde{x}}{Dt} = \frac{\tilde{\Gamma}}{\bar{\rho}} \tag{4}$$

where Γ is the vapour generation rate, x is the vapour quality. The total enthalpy defined in Eq. (5) is a sum of the specific enthalpy and the kinetic energy:

$$\tilde{E} = \tilde{h} + \frac{\tilde{u}^2}{2} \tag{5}$$

where h is the specific enthalpy. According to Downar-Zapolski et al. (1996), the specific enthalpy and the total density of the mixture can be defined as follows:

$$\tilde{h} = \tilde{x} \cdot \tilde{h}_{sv} + (1 - \tilde{x}) \cdot \tilde{h}_{ml} \tag{6}$$

$$\bar{\rho} = \tilde{\alpha} \cdot \bar{\rho}_{sv} + (1 - \tilde{\alpha}) \cdot \bar{\rho}_{ml}\left(\bar{p}, \tilde{h}_{ml}\right) \tag{7}$$

where h_{ml} and ρ_{ml} are the specific enthalpy and the density in metastable conditions, respectively, h_{sv} and ρ_{sv} are the specific enthalpy and the density of the saturated vapour, respectively, α is the void fraction of the mixture. The void fraction is the local quality of the mixture multiplied by the ratio of the local density and the density of the saturated vapour:

$$\tilde{\alpha} = \frac{\tilde{x} \cdot \bar{\rho}}{\bar{\rho}_{sv}} \tag{8}$$

The vapour mass balance equation presented in Eq. (4) can be defined based on a linearised expansion proposed by Bilicki and Kestin (1990):

$$\frac{D\tilde{x}}{Dt} = -\frac{\tilde{x} - \tilde{x}_{eq}}{\tilde{\theta}} \tag{9}$$

where x and x_{eq} are the instantaneous and the equilibrium quality and θ is RT. According to Downar-Zapolski et al. (1996), RT for low pressure (up to 10 bar for water) can take the form:

$$\tilde{\theta} = \theta_{0,1} \cdot \tilde{\alpha}^{a_1} \cdot \bar{\psi}^{b_1} \tag{10}$$

where $\theta_{0,1}$ is the constant reference RT of 6.51e-04 s, a_1 and b_1 are the constant coefficients set to -0.257 and -2.24, respectively, and ψ is the non-dimensional pressure difference, which is given below:

$$\bar{\psi} = \left| \frac{\bar{p}_{sat}(T_{motive}) - \bar{p}}{\bar{p}_{sat}(T_{motive})} \right| \tag{11}$$

where p_{sat} is the saturation pressure at given motive nozzle temperature T_{motive}. RT for higher pressures with the constant coefficients for R744 is defined in the work of (Angielczyk et al., 2010) in the following manner:

$$\tilde{\theta} = \theta_{0,2} \cdot \tilde{\alpha}^{a_2} \cdot \bar{\varphi}^{b_2} \tag{12}$$

where $\theta_{0,2}$ is the constant reference RT of 2.14e-07 s, a_2 and b_2 are set to -0.54 and -1.76, respectively, and φ is the other form of the non-dimensional pressure difference adapted for the supercritical parameters (Angielczyk et al., 2010):

$$\bar{\varphi} = \left| \frac{\bar{p}_{sat}(s_{motive}) - \bar{p}}{p_{crit} - \bar{p}_{sat}(s_{motive})} \right| \tag{13}$$

where p_{crit} is the critical pressure of CO_2, s_{motive} is the motive nozzle specific entropy and p_{sat} is the saturation pressure at the given motive nozzle specific entropy. The saturation pressure defined by the given motive nozzle specific entropy allows for the calculation of the non-dimensional pressure difference φ for the motive nozzle temperature above the critical temperature. The determination of the saturation pressure was shown in Figure 1.

The formulation of RT led to investigation of the correlation of the relaxation time and the local parameters of the two-phase flow. RT was analysed either as a constant value or for different values of the constant coefficients. The HRM approach was implemented with the numerical model of the two-phase ejector. The numerical simulations of the R744 two-phase flow led to calculation of the two-phase flow behaviour as well as the ejector performance, which describes the possibility of the suction nozzle flow entrainment by the expanded motive nozzle flow at increase of the mixed flow pressure. The mass entrainment ratio ϕ is the ejector performance parameter defined as a ratio of the suction MFR and the motive MFR:

$$\phi = \frac{\dot{m}_{suction}}{\dot{m}_{motive}} \tag{14}$$

The pressure lift is the ejector specific parameter, which shows the difference of the outlet pressure and the suction nozzle pressure expressed as:

$$dP = P_{outlet} - P_{suction} \tag{15}$$

The foregoing parameters were used to define the different operating conditions of the two-phase ejector to perform the modified HRM investigation for ejector performance. The accuracy of the modified HRM was investigated based on the experimental data.

3 Test campaign

The modified HRM investigation was performed based on the designed R744 two-phase ejector presented in Figure 2. The ejector was implemented in the multi-ejector module, which was designed to ensure the maximum system flexibility at different ambient temperatures and cooling capacities of the refrigeration system (Banasiak et al., 2015). The set of the main geometry parameters of the designed ejector installed in the multi-ejector module is presented in Table 1.

The operating conditions presented in Table 2 were set for typical supermarket refrigeration applications. The defined points were selected to perform the analysis in the region for which HEM and HRM with RT defined in the literature obtained both high and low accuracy of the motive and suction mass flow rates (Palacz et al., 2017a). The motive nozzle pressure varied from 50 bar to 95 bar. The numerical investigation is performed for either trans-critical conditions or subcritical conditions linked to the ambient temperature. The suction nozzle pressure is related to the evaporation temperature in the medium-temperature evaporator between -10 °C and -6 °C. The outlet conditions were set to analyse the accuracy of the HRM model for different values of the pressure lift. For clarity, the motive and suction nozzle conditions were also presented on *p-h* diagram in Figure 3.

The set of the operating conditions presented in Table 2 was used to validate the modified HRM results based on the experimental data carried out at SINTEF Energy Research laboratory in Trondheim, Norway. The modification of the RT formulation was performed to minimise the discrepancy of the modified HRM motive nozzle MFR compared to the experimental data.

4 Computational procedure for the relaxation time modification

The numerical investigation was performed using the commercial ANSYS software on the *ejectorPL* platform (Palacz et al., 2015). The purpose of the *ejectorPL* software is to automate the simulation process by combining and controlling the geometry together with the mesh generator ANSYS ICEM CFD, executing the solver in ANSYS Fluent for the flow simulation, and finally processing the results data for the ejector operation. The *ejectorPL* is modified for the different constant coefficients of the RT correlation.

The partial differential equations of the mathematical model were solved based on the PRESTO scheme for the pressure discretisation and the second-order upwind scheme for the other variables considered in the CFD model. The coupled method was employed for the coupling of the pressure and velocity fields. The 2-D axisymmetric ejector geometry was

discretised with a fully structured grid of less than 10,000 elements with a minimum orthogonal quality of 0.9. The wall roughness was set to 2 μm according to the ejectors manufacturers (Banasiak and Hafner, 2013). The ejector mesh independence study was provided in the previous studies where the discretisation process was also presented (Smolka et al. (2013) and Palacz et al. (2016)). The real fluid properties of R744 were approximated based on data obtained using the REFPROP libraries (Lemmon et al., 2013).

The *k-ω* SST model was used to model the turbulent flow inside the ejector (Fluent, 2011). According to Mazzelli et al. (2015), the *k-ω* SST model showed the best agreement of the global and local flow parameters inside the ejector. Hence, the foregoing turbulence model was applied into the CFD model to simulate the flow behaviour inside the R744 two-phase ejector. During the numerical investigation of the modified HRM, the *k-ω* SST model properly predicted the mixing process of both streams inside the pre-mixer and the mixing chamber. Moreover, the turbulence model indicated local flow vortex for the operating conditions with the high pressure lift. Hence, the mass entrainment possibility of the motive nozzle stream was very low or even negligible.

The CFD simulations were performed in two steps. Firstly, the HEM calculations were computed. The convergence criterion was reached when the MFR imbalance was below 1% and both motive nozzle and suction nozzle MFRs were stabilised. When the HEM calculations obtained the convergence criterion, the HRM computations were performed until the similar convergence criterion was reached. In this manner, the convergence problems for all the investigated operating points were not observed.

The accuracy of the selected parameter of the numerical model was calculated as the relative error between the experimental (exp) and the numerical results (num) of the motive nozzle MFR or the suction nozzle MFR.

$$\delta_{\dot{m}} = \frac{\dot{m}_{exp} - \dot{m}_{num}}{\dot{m}_{exp}} \cdot 100\% \tag{16}$$

where $\delta_{\dot{m}}$ is the relative error, $\dot{m}$ is the motive nozzle MFR or the suction nozzle MFR given by the experimental data or the numerical results. The acceptable relative difference between the experimental and the numerical results was assumed as less than or equal to 10%.

The RT formulation was modified by the change of the constant coefficients. In the first step, RT was defined as a constant value throughout the ejector to evaluate the influence of the relaxation on the motive stream expansion process and the mixing process in the mixing

section. The mapping of each RT constant coefficient was performed by use of a genetic algorithm, which had been applied for a shape optimisation (Corriveau et al., 2010; Gallegos Muñoz et al., 2011; Smolka, 2013a, b). The genetic algorithm was implemented on the *ejectorPL* platform to perform the mixer-shape optimisation and the ejector-shape optimisation by Palacz et al. (2016); (2017b). The aim of the genetic algorithm application was to minimise the objective function (OF), which is the motive nozzle MFR discrepancy for the selected number of the cases presented in Table 2.

$$OF(\theta_0, a, b) = \frac{1}{n}\sum_{i=1}^{n} \delta_{\dot{m}_{motive,i}} \rightarrow min \tag{17}$$

where n is the total number of selected cases. The population size was 10 individuals per generation. The uniform crossover between the individuals, jump mutations and creep mutations were performed with a probability equal to 0.5, 0.02 and 0.04. Elitism strategy was used to keep the best individual. The optimal solution was obtained after approximately 20 generations. The GA executes the following steps:

1. The control program executes the GA, which generates a population of constants defined relaxation time parameters
2. The population of sets of relaxation time constants parameters is input to the computational tool (*ejectorPL*)
3. The control program obtains the solutions for all individuals in the population, where solutions are obtained for each of the chosen operating conditions
4. The control code ensures that all of the computational tool processes have finished
5. The computational tool calculates the discrepancy of the motive nozzle MFR for the all considered OCs and the all individuals
6. The GA processes the computational results to calculate and then evaluate the objective function OF
7. The RT constants of the best individual (highest OF value) are saved
8. The control code goes to Step 1

The constant coefficients described the RT correlation in Eq. (12) were considered in the optimisation procedure to minimise the discrepancy of the modified HRM against the experimental data. The variation range for each selected parameter was set in the following ranges: $\theta_0 \in \langle 5.0e-08; 1.0e-05\rangle$, $a \in \langle -1; -0.5\rangle$, $b \in \langle -2; -1.5\rangle$. The number of possibilities was 50 for each optimised parameter.

The investigation of the RT modification was performed either for the constant value or by use of the genetic algorithm to improve the modified HRM accuracy compared to HEM and HRM with the RT correlation presented by Downar-Zapolski et al. (1996) and Angielczyk et al. (2010) at specific operating conditions.

5 The RT constants investigation

In this section, the RT constants investigation are presented and discussed. The influence of the different RT constant θ_0 on R744 two-phase flow behaviour compared to the HEM results is analysed in Section 5.1. The analysis of the exponent *a* in Eq. (12) was discussed in Section 5.2. The influence of the exponent *b* in Eq. (12) was presented in Section 5.3.

5.1 RT constant

The different RT constant θ_0 values influenced the expansion process and mixing process in the R744 two-phase flow. Figure 4 presents the pressure distribution along the axis of the two-phase ejector at the operating conditions represented by three motive nozzle pressure levels in subcritical and trans-critical regimes. The pressure distribution is shown for the HEM results and for the RT constant θ_0 in the range from 10^{-6} s to 10^{-3} s related to the HRM investigation of the R744 two-phase flow inside the pipelines for different θ_0 presented by Brown et al. (2013). The increase of RT decreased the pressure in the diverging part. The pressure level at the end of the motive nozzle is lower for HRM compared to HEM. Moreover, HRM indicated the shock wave close to the motive nozzle outlet. The expansion waves were generated earlier in HRM; therefore, for the high relaxation time both streams were well mixed in the mixer due to stabilisation of the flow velocity. The pressure difference of HEM and HRM for relaxation time above 10^{-5} s after the throat was 5 bar, 13 bar, and 5 bar at OC #2, #11, and #20. The metastable effect decreased the pressure in the motive converging-diverging nozzle, which resulted in the increase of the critical MFR.

Figure 5 presents the vapour quality distribution along the axis of the two-phase ejector at the operating conditions presented in Figure 4. Similar to the pressure distribution, the vapour quality distribution is shown for the HEM results and for the constant relaxation time in the range from 10^{-6} s to 10^{-3} s. The increase of RT constant θ_0 delayed the evaporation of the

motive stream. The vapour quality distribution is close to the HEM results for RT below 10^{-5} s. For θ_0 of 10^{-3} s the motive stream slightly evaporated through the pre-mixing chamber and the mixer. RT above 10^{-5} s influenced the mixing process; thereby the mixed stream obtained the equilibrium state far from the beginning of the mixing section. In the motive nozzle, the metastable effect delayed the evaporation of the motive stream. Therefore, the density increased in the motive nozzle due to the superheated liquid flow through the nozzle and the decrease of the pressure distribution during the increase of RT constant θ_0.

Figure 6 presents the velocity field of the motive nozzle, suction nozzle, pre-mixing chamber and the mixer for different specified RT constant θ_0 at the operating condition #6 listed in Table 2. The velocity of the motive stream decreased rapidly after the first shock as a result of RT increase. The velocity profile for RT of 10^{-6} s is similar to the velocity profile obtained by HEM as a result of the metastable effect omission. The motive stream in the diverging part of the motive nozzle accelerated faster when RT constant was increased as a result of the higher influence of the metastability. However, the maintenance of RT constant θ_0 above 10^{-4} s in the mixer caused the motive stream to slow down, which affected the lower entrainment of the suction stream. Therefore, RT constant θ_0 correlation defined as a function of the void fraction and the non-dimensional pressure difference led to determining the real metastable region inside the ejector. The different behaviours of the two-phase flows inside the ejector for either subcritical or trans-critical operating conditions force setting different relaxation time coefficients at different motive nozzle pressure ranges.

5.2 Exponent *a*

The exponent *a* in Eq. (12) determines the influence of the local void fraction value on the relaxation time. Hence, the parametrisation procedure of the exponent *a* was performed to analyse the accuracy of the HRM motive nozzle MFR. Figure 7 presents the motive nozzle MFR discrepancy of HRM for different exponents *a* in the range from -3.0 to 1.0 at OC #12 defined in Table 2. Based on the results presented in Section 5.1, the investigation was performed for two different RT constants $\theta_0$in Eq. (12). The exponent *b* in Eq. (12) was set to -1.56 according to Angielczyk et al. (2010). The HRM motive nozzle MFR discrepancy slightly varied in the range from approximately 21% to 23% for RT constant θ_0 of 2.14e-07 s. The best HRM accuracy of approximately 4.0% was obtained for the exponent *a* of -1.0 and

RT constant θ_0 of 7.0e-06. It can be seen that the increase of the RT constant θ_0 showed higher influence of the void fraction parameter on the HRM accuracy. Therefore, the increase of the exponent *a* above -1.00 increased the motive nozzle MFR discrepancy of HRM.

Figure 8 presents the contour plots of the HRM absolute pressure in the diverging part of the motive nozzle, suction nozzle and mixing section for different constants presented in Eq. (12) at OC #12 defined in Table 2. The exponent *a* was defined as -1.5 and -1.0 for RT constant θ_0 of 2.14e-07 s and of 7.00e-06 s. The exponent b was set to -1.56 according to Angielczyk et al. (2010). The negligible influence of the void fraction parameter can be observed for low value of the RT constant θ_0 due to local low value of the relaxation time. The increase of the RT constant θ_0 decreased the local absolute pressure value in the diverging part of the motive nozzle. Moreover, the change of the exponent *a* from -1.5 to -1.0 reduced the shock waves in the pre-mixing chamber for RT constant θ_0 of 2.14e-06 s. Moreover, the pressure increased earlier in the mixing section for RT constant θ_0 of 7.00e-06 s. Hence, the change of the exponent *a* influenced on the mixing process of both streams.

5.3 Exponent *b*

The non-dimensional pressure difference parameter influenced the relaxation time value based on the local pressure value compared to the saturation pressure and the critical pressure. Therefore, the parametrisation procedure of the exponent b presented in Eq. (12) was performed. Figure 9 presents the HRM motive nozzle MFR discrepancy for different exponents *b* in the range from -3.0 to 1.0 at the operating conditions #12 defined in Table 2. In similar to the results presented in Figure 7, the investigation was performed for two different RT constants θ_0. The value of the exponent *a* was set to -0.54 according to Angielczyk et al. (2010). The discrepancy of HRM was in the range from approximately 27% to 32% for RT constant θ_0 of 2.14e-07 s and the lowest accuracy was obtained for *b* of -1.25. The highest HRM motive nozzle MFR accuracy of approximately 6% was reached for the exponent *b* of -1.76 and RT constant θ_0 of 7.0e-06 s. The increase of *b* above -1.75 increased the HRM discrepancy up to approximately 21% for *b* of 1.

The influence of the exponent *b* value on the absolute pressure field of HRM in the diverging part of the motive nozzle, the suction nozzle and the mixing-section was presented in Figure 10. The analysis was performed for two exponents *b* of -1.5 and -1.0 at the operating conditions #13 presented in Table 2. Similar to the investigation of the exponent *a* presented in Figure 8 the RT constant θ_0 was set to 2.14e-07 s and 7.00e-06 s. The exponent *a* was defined as -0.54 according to Angielczyk et al. (2010). It can be observed that the change of *b* obtained slightly different local values of the absolute pressure at the end of the motive nozzle and in the pre-mixing chamber for RT constant θ_0 of 2.14e-07 s. Hence, the increase of the RT constant θ_0 up to 7.0e-06 s increased the pressure in the diverging part of the motive nozzle. Moreover, the exponent *b* of -1.0 obtained higher local values of the absolute pressure in the motive nozzle and insignificant pressure difference in the pre-mixer when compared to *b* of -1.5. In the mixer, the absolute pressure increased for *b* of -1.0 when compared to the *b* of -1.5 for the RT constant θ_0 of 7.00e-06 s.

The investigation of each constants presented in Eq. (12) indicated different global and local values of the two-phase flow parameters inside the R744 related to the influence on the relaxation time. The proper modifications of the constants for different operating regimes allows for the improvement of the modified HRM and the application range extension in the subcritical region.

6 Modified HRM validation

The RT constants investigation indicated high influence of the RT value on the expansion process in the motive nozzle and the mixing process in the pre-mixing chamber as well as in the mixer. Therefore, the RT correlation should increase the influence of the metastable effect in the subcritical operating regime and simultaneously omit the evaporation delay in the trans-critical operating regime. The modification of the RT correlation was performed by use of the genetic algorithm to optimise the values of the RT coefficients presented in Eq. (12). The modified HRM was optimised for three selected pressure ranges, depending on the influence of the metastable effect on the motive stream evaporation process delay. The subcritical

region was defined for two pressure ranges either above 59 bar or below 59 bar to take into consideration the motive flow evaporation delay for proper motive nozzle pressure level. The optimised relaxation time coefficients as well as minimum value of the objective function for each selected motive nozzle pressure range are listed in Table 3. In addition, the optimisation procedure of each pressure range was performed for four selected operating conditions presented in Table 2 to investigate the modified HRM accuracy at a wide range of operating conditions and minimise the computational time of the optimisation procedure. The lowest OF was obtained for trans-critical operating conditions due to negligible influence of the metastable effect.

Figure 11 shows the motive nozzle MFR discrepancy of the investigated CFD models at the operating conditions above the critical point. The results given by HEM and HRM with the RT correlation defined by Angielczyk et al. (2010) and Downar-Zapolski et al. (1996) were compared to the modified HRM results. Each investigated numerical model obtained accuracy within ±10%. The HEM results overestimated the motive nozzle MFR for the motive nozzle pressure above 85 bar compared to the experimental data. The discrepancy of HEM was below 5% at operating points close to the critical point. HRM with RT correlation presented in Eq. (12) increased the motive nozzle MFR at each investigated point. Hence, the HRM reached higher discrepancy of the motive nozzle MFR than HEM for motive nozzle pressure above 85 bar. In addition, the motive nozzle MFR of HRM based on the RT correlation presented by Angielczyk et al. (2010) was overestimated at OC #3 compared to the experimental data. The motive nozzle MFRs of HRM with RT correlation presented by Downar-Zapolski et al. (1996) were overestimated for each investigated point besides OC #7 compared to the experimental results. The modified HRM had similar results to HEM. The modified HRM motive nozzle MFR accuracy was similar to HEM in the trans-critical operating regime.

The suction nozzle MFR discrepancy of each investigated CFD model at the operating conditions above critical point is shown in Figure 12. The HEM results had a discrepancy below 10% at OC #1 and #7. The highest suction nozzle MFR discrepancy was approximately 32%. The different relaxation time correlations significantly influenced the suction MFR. HRM with RT correlation defined in Eq. (12) had a discrepancy of approximately 40% at OC #3 and #6. The suction nozzle MFR discrepancy of HRM with RT presented by Downar-

Zapolski et al. (1996) was in the range of approximately 12% to 35%. The suction nozzle MFR accuracy of the modified HRM varied in the range of 15% to approximately 25%. Therefore, the modified HRM obtained underestimated MFR of the suction stream for the motive nozzle pressure above the critical point compared to the experimental data as the result of the defined turbulence model.

The motive nozzle MFR accuracy of HEM, HRM with the literature relaxation time correlations and modified HRM at the operating conditions in the range of 59 bar to the critical point are shown in Figure 13. The HEM motive nozzle MFR discrepancy was over 15% at each investigated point. Decreasing the motive nozzle pressure range increased the underestimation of the HEM motive nozzle flow. The HRM results with the RT correlation presented by Angielczyk et al. (2010) improved the model accuracy compared to HEM. Although the HRM discrepancy was over 15% for OC #9, #12 and #13, HRM with the RT correlation defined by Downar-Zapolski et al. (1996) had better accuracy compared to HEM and HRM with the RT correlation defined by Angielczyk et al. (2010). The best accuracy was obtained by the modified HRM at each investigated operating point. The modified HRM discrepancy of the motive nozzle MFR was below 10% for motive nozzle pressure in the range from 60 bar to 68 bar. The modified HRM was accurate below 15% at OC #13. The optimisation of the RT coefficients in the modified HRM led to numerical investigation of the R744 two-phase ejector with the highest accuracy of the CFD model at motive nozzle pressure above 58 bar.

Figure 14 presents the suction nozzle MFR discrepancy of HEM and HRMs at the motive nozzle pressure in the range of 59 bar to the critical point. The HEM results had a similar entrained flow at OC #9 compared to the experimental data. However, the HEM accuracy of the suction nozzle MFR was in the range of 15% to 30% at the remaining operating points. HRM with RT correlation presented by Angielczyk et al. (2010) overestimated the entrained flow at OC #9; the discrepancy was approximately -20%. The HRM obtained similar suction nozzle MFR accuracy compared to HEM at OC #10, #12 and #13. At OC #11, the suction nozzle MFR discrepancy was approximately 20%. The discrepancy of HRM with RT presented by Downar-Zapolski et al. (1996) was in the range of approximately 5% to 30% at OC #10, #11 and #12. The entrained stream was overestimated by the HRM at OC #9 and

#13; the accuracy was -50% and approximately -1%. The high overestimation of the suction MFR by both HRMs was obtained due to the high pressure lift and a very small ϕ. The suction nozzle MFR discrepancy of the modified HRM varied in a range from 10% to approximately 20% at OC #9, #12 and #13. The underestimation of the entrained flow over 40% was obtained at OC #10 and #11.

The motive nozzle MFR accuracy of the investigated numerical models for the motive nozzle pressure below 59 bar is presented in Figure 15. The HEM motive nozzle MFR discrepancy was over 20% at each investigated point. The lowest HEM motive nozzle MFR accuracy was approximately 40% at OC #22. The HRM results for RT defined by the literature correlations took into account the influence of the metastable effect on the motive nozzle flows similar to each other. Therefore, the accuracy of both relaxation models was higher compared to HEM by up to approximately 5%. The optimised RT correlation had the best improvement of the motive nozzle MFR accuracy at each investigated operating condition. The modified HRM had lower motive nozzle MFR discrepancy compared to HRM with the literature RT correlations in the range from 2% to 5%. However, the discrepancy obtained by the modified HRM was still above 10% at each operating point. The modified HRM improved the accuracy of the motive nozzle MFR compared to the HEM approach by 5% to 10%, but the assumed homogenous relaxation flow was not able to predict the real fluid flow.

The suction nozzle MFR discrepancy of each investigated CFD model at the operating conditions below 59 bar is shown in Figure 16. HEM had a discrepancy of over 35% at each operating point. The HRM suction nozzle MFR discrepancy with RT defined in Eq. (12) was over 30% at OC #14, #16, #18, #20, #21 and #22. The HRM significantly overestimated the suction nozzle MFR at #15 and #19. The best accuracy was obtained at OC #17 slightly below 15%. The HRM suction nozzle MFR accuracy with the RT correlation presented by Downar-Zapolski et al. (1996) was similar to the HEM accuracy at OC #16, #17 #18, #20 and #22. In addition, the overestimation of the entrainment flow was reached at OC #14, #15 and #19 and the discrepancy was below -15% for #15 and #19. At OC #21, the numerical model had accuracy below 5%. The modified HRM underestimated the entrained stream at each operating point. The suction nozzle MFR accuracy of the modified HRM was below 15% at OC #14, #15 and #17. Therefore, the modified HRM obtained the best suction nozzle mass

flow rate prediction for the motive nozzle pressure below 59 bar compared to HEM and HRMs with the RT correlation presented in the literature.

Figure 17 presents the motive and suction nozzle MFR discrepancies of the modified HRM on the pressure-specific enthalpy diagram. The best accuracy of the motive nozzle MFR presented in Figure 17(a) was obtained in the transcritical regime close to the critical temperature. In the subcritical region, the discrepancy of the modified HRM motive nozzle MFR was below 5% above 60 bar and close to the saturation line. In the subcritical region below 60 bar, the accuracy of the modified HRM decreased and the motive nozzle MFR discrepancy was over 20% for most investigated points. The suction nozzle MFR discrepancy of the modified HRM was presented in Figure 17(b). The best accuracy was obtained for operating points with high superheat. The highest suction nozzle MFR discrepancy was of 100% due to the high pressure lift and the suction stream of the modified HRM was not entrained by the motive stream. The accuracy of the modified HRM for suction nozzle pressure in the range from 30 bar to 35 bar was differentiated according to the defined pressure lift..

The improvement of the modified HRM accuracy was obtained due to the significant increase of the meta-stability influence on the expansion process in the converging-diverging motive nozzle. Figure 18 presents the expansion process of the motive stream of HEM and the modified HRM on the pressure-specific enthalpy diagram and the pressure-specific volume diagram. The fluid flow parameters in the throat of both CFD models are marked on the diagrams. The modified HRM expanded much deeper in the high-pressure stream in the motive nozzle. Hence, the modified HRM motive nozzle flow reached the pressure level of approximately 43 bar in the throat, where the HEM motive nozzle flow reached a pressure level up to 50 bar. The motive nozzle stream expanded for HEM and the modified HRM up to approximately 27 bar and 23 bar.

The lower pressure of the modified HRM high-pressure stream in the converging-diverging nozzle and the relaxation of the motive flow indicated much lower specific volume compared to HEM flow through the motive nozzle. The foregoing effects increased the density of the motive stream especially in the throat, thereby the motive nozzle MFR increased depending on RT. The influence of the meta-stability effect can be observed right after the liquid saturation line and around the throat. The modified HRM flow had shock wave generation at

the end of the converging-diverging nozzle because of the effect of the high pressure difference in the mixing section.

7 Conclusions

The numerical investigation of the proposed modified HRM of the R744 two-phase ejector was performed based on the analysis of the motive nozzle MFR accuracy and mass entrainment ratio accuracy. The MFRs given by the CFD results were compared to the experimental results. The RT correlation of the modified HRM was optimised based on the developed genetic algorithm integrated with the *ejectorPL* platform. The influence of the three RT constants values on ejector performance was analysed. The CFD results of the modified HRM were compared to the HEM results and HRM models with different relaxation time correlations given by the literature.

An increase of the RT constant θ_0 delayed the evaporation process of the motive high pressure liquid stream. Therefore, the value of RT above 10^{-4} s significantly decreased the quality and the pressure of the motive fluid in the converging-diverging nozzle independently of the operating conditions. However, RT strongly influenced the shock wave generations and the mixing process in the pre-mixing chamber and the mixer. RT above 10^{-4} s slowed down the motive stream in the mixing section, which affected the ejector performance. The modifications of the exponents a and b influenced the global and local values of the two-phase flow at different RT constant θ_0. Hence, the modification of each RT constants at selected operating regime let to improve the accuracy of the modified HRM.

The modified HRM obtained the best accuracy of the motive nozzle MFR for the subcritical operating regimes compared to HEM and the other HRM models based on different literature relaxation time correlations. For the trans-critical operating regimes, the small constant relaxation time value in the modified HRM limited the metastable effect of the two-phase flow. As a result, the modified HRM results had similar accuracy compared to the HEM results. The application range of the modified HRM was extended to 59 bar for the motive nozzle pressure. The resulting motive nozzle MFR discrepancy was below 15% for the investigated operating conditions. The suction nozzle MFR accuracy of the modified HRM was similar to HEM at most of the investigated operating points. For the motive nozzle pressure level below 59 bar, the modified HRM improved the accuracy of the motive MFR in

the range of 5% to 10% compared to HEM and HRMs with RT correlations given by literature.

Acknowledgment

The authors gratefully acknowledge the financial support of the Research Council of Norway through project No. 244009/E20.

Reference

Angielczyk, W., Bartosiewicz, Y., Butrymowicz, D., Seynhaeve, J.-M., 2010. 1-D Modeling Of Supersonic Carbon Dioxide Two-Phase Flow Through Ejector Motive Nozzle International Refrigeration and Air Conditioning Conference. Purdue e-Pubs, Purdue University.

Banasiak, K., Hafner, A., 2013. Mathematical modelling of supersonic two-phase R744 flows through converging–diverging nozzles: The effects of phase transition models. Appl. Therm. Eng. 51, 635-643.

Banasiak, K., Hafner, A., Andresen, T., 2012. Experimental and numerical investigation of the influence of the two-phase ejector geometry on the performance of the R744 heat pump. Int. J. Refrigeration 35, 1617-1625.

Banasiak, K., Hafner, A., Kriezi, E.E., Madsen, K.B., Birkelund, M., Fredslund, K., Olsson, R., 2015. Development and performance mapping of a multi-ejector expansion work recovery pack for R744 vapour compression units. Int. J. Refrigeration 57, 265-276.

Besagni, G., Inzoli, F., 2017. Computational fluid-dynamics modeling of supersonic ejectors: Screening of turbulence modeling approaches. Appl. Therm. Eng. 117, 122-144.

Bilicki, Z., Kestin, J., 1990. Physical Aspects of the Relaxation Model in Two-Phase Flow. Proceedings of the Royal Society of London A: Mathematical, Physical and Engineering Sciences 428, 379-397.

Brown, S., Martynov, S., Mahgerefteh, H., Proust, C., 2013. A homogeneous relaxation flow model for the full bore rupture of dense phase CO2 pipelines. Int. J. Greenh. Gas Control 17, 349-356.

Colarossi, M., Trask, N., Schmidt, D.P., Bergander, M.J., 2012. Multidimensional modeling of condensing two-phase ejector flow. Int. J. Refrigeration 35, 290-299.

Corriveau, G., Guilbault, R., Tahan, A., 2010. Genetic algorithms and finite element coupling for mechanical optimization. Advances in Engineering Software 41, 422-426.

Deng, J.q., Jiang, P.x., Lu, T., Lu, W., 2007. Particular characteristics of transcritical CO2 refrigeration cycle with an ejector. Appl. Therm. Eng. 27, 381-388.

Downar-Zapolski, P., Bilicki, Z., Bolle, L., Franco, J., 1996. The non-equilibrium relaxation model for one-dimensional flashing liquid flow. International Journal of Multiphase Flow 22, 473-483.

Elbel, S., Hrnjak, P., 2008. Experimental validation of a prototype ejector designed to reduce throttling losses encountered in transcritical R744 system operation. Int. J. Refrigeration 31, 411-422.

Elbel, S., Lawrence, N., 2016. Review of recent developments in advanced ejector technology. Int. J. Refrigeration 62, 1-18.

Fluent, A., 2011. Ansys Fluent User's Guide. PA, Canonsburg.

Gallegos Muñoz, A., Ayala-Ramírez, V., Alfaro-Ayala, J.A., Toledo Acosta, B.M., 2011. Optimization of the transition piece applying genetic algorithms. Appl. Therm. Eng. 31, 3214-3225.

Giacomelli, F., Biferi, G., Mazzelli, F., Milazzo, A., 2016. CFD Modeling of the Supersonic Condensation Inside a Steam Ejector. Energy Procedia 101, 1224-1231.

Hafner, A., Forsterling, S., Banasiak, K., 2014. Multi-ejector concept for R-744 supermarket refrigeration. Int. J. Refrigeration 43, 1-13.

Haida, M., Banasiak, K., Smolka, J., Hafner, A., Eikevik, T.M., 2016. Experimental analysis of the R744 vapour compression rack equipped with the multi-ejector expansion work recovery module. Int. J. Refrigeration 64, 93-107.

Kornhauser, A.A., 1990. The Use of an Ejector as a Refrigerant Expander, International Refrigeration and Air Conditioning Conference. Purdue e-Pubs, Purdue University, p. 11.

Lemmon, E.W., Huber, M.l., McLinden, M.O., 2013. NIST Standard Reference Database 23: Reference Fluid Thermodynamic and Transport Properties-REFPROP, Standard Reference Data Program, 9.1 ed. National Institute of Standards and Technology, Gaithersburg.

Li, D., Groll, E.A., 2005. Transcritical CO2 refrigeration cycle with ejector-expansion device. Int. J. Refrigeration 28, 766-773.

Lorentzen, G., 1990. Trans-critical vapour compression cycle device. Google Patents.

Lucas, C., Rusche, H., Schroeder, A., Koehler, J., 2014. Numerical investigation of a two-phase CO2 ejector. Int. J. Refrigeration 43, 154-166.

Mazzelli, F., Little, A.B., Garimella, S., Bartosiewicz, Y., 2015. Computational and experimental analysis of supersonic air ejector: Turbulence modeling and assessment of 3D effects. International Journal of Heat and Fluid Flow 56, 305-316.

Nakagawa, M., Berana, M.S., Kishine, A., 2009. Supersonic two-phase flow of CO2 through converging–diverging nozzles for the ejector refrigeration cycle. Int. J. Refrigeration 32, 1195-1202.

Palacz, M., Haida, M., Smolka, J., Nowak, A.J., Banasiak, K., Hafner, A., 2017a. HEM and HRM accuracy comparison for the simulation of CO2 expansion in two-phase ejectors for supermarket refrigeration systems. Appl. Therm. Eng.

Palacz, M., Smolka, J., Fic, A., Bulinski, Z., Nowak, A.J., Banasiak, K., Hafner, A., 2015. Application range of the HEM approach for CO2 expansion inside two-phase ejectors for supermarket refrigeration systems. Int. J. Refrigeration.

Palacz, M., Smolka, J., Kus, W., Fic, A., Bulinski, Z., Nowak, A.J., Banasiak, K., Hafner, A., 2016. CFD-based shape optimisation of a CO2 two-phase ejector mixing section. Appl. Therm. Eng. 95, 62-69.

Palacz, M., Smolka, J., Nowak, A.J., Banasiak, K., Hafner, A., 2017b. Shape optimisation of a two-phase ejector for CO2 refrigeration systems. Int. J. Refrigeration 74, 210-221.

Salvador, F.J., Carreres, M., Jaramillo, D., Martínez-López, J., 2015. Comparison of microsac and VCO diesel injector nozzles in terms of internal nozzle flow characteristics. Energy Convers. Manag. 103, 284-299.

Schmidt, D.P., Gopalakrishnan, S., Jasak, H., 2010. Multi-dimensional simulation of thermal non-equilibrium channel flow. International Journal of Multiphase Flow 36, 284-292.

Smolka, J., 2013a. CFD-based 3-D optimization of the mutual coil configuration for the effective cooling of an electrical transformer. Appl. Therm. Eng. 50, 124-133.

Smolka, J., 2013b. Genetic algorithm shape optimisation of a natural air circulation heating oven based on an experimentally validated 3-D CFD model. Int. J. Therm. Sci. 71, 128-139.

Smolka, J., Bulinski, Z., Fic, A., Nowak, A.J., Banasiak, K., Hafner, A., 2013. A computational model of a transcritical R744 ejector based on a homogeneous real fluid approach. Applied Mathematical Modelling 37, 1208-1224.

Sumeru, K., Nasution, H., Ani, F.N., 2012. A review on two-phase ejector as an expansion device in vapor compression refrigeration cycle. Renew. Sustain. Energy Rev. 16, 4927-4937.

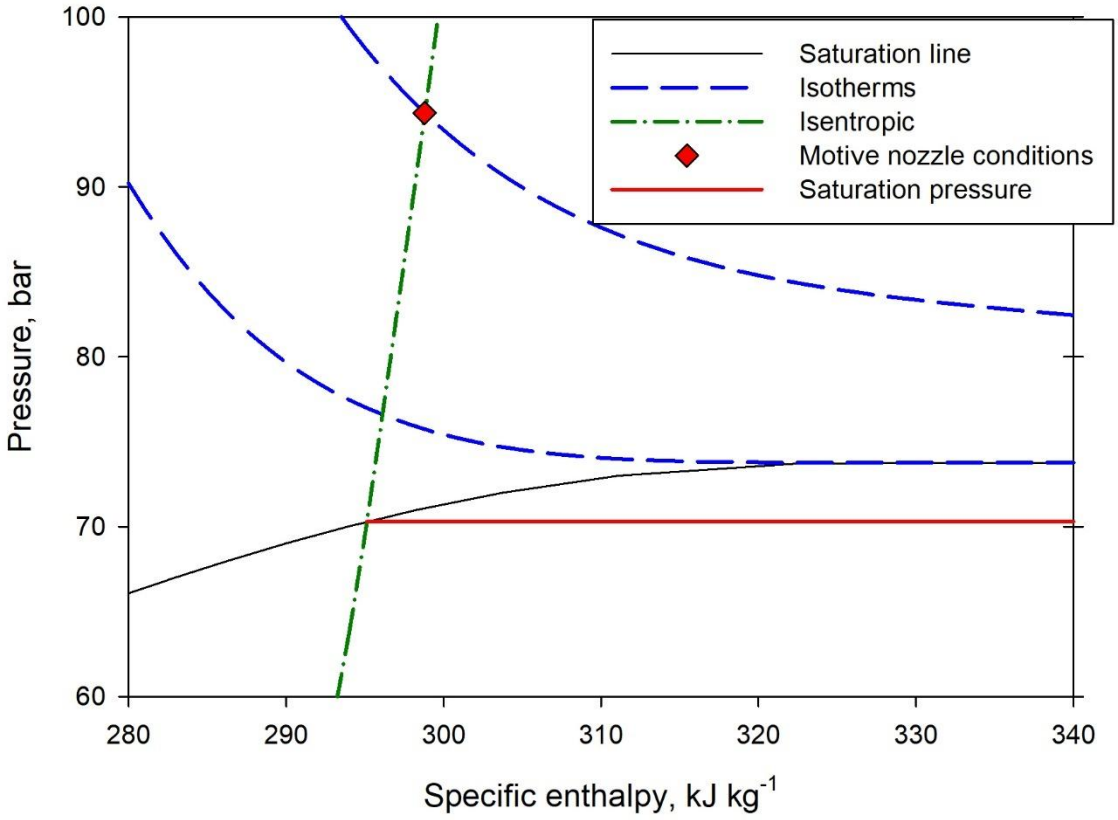

Figure 1 Saturation pressure determination of the transcritical motive nozzle operating conditions.

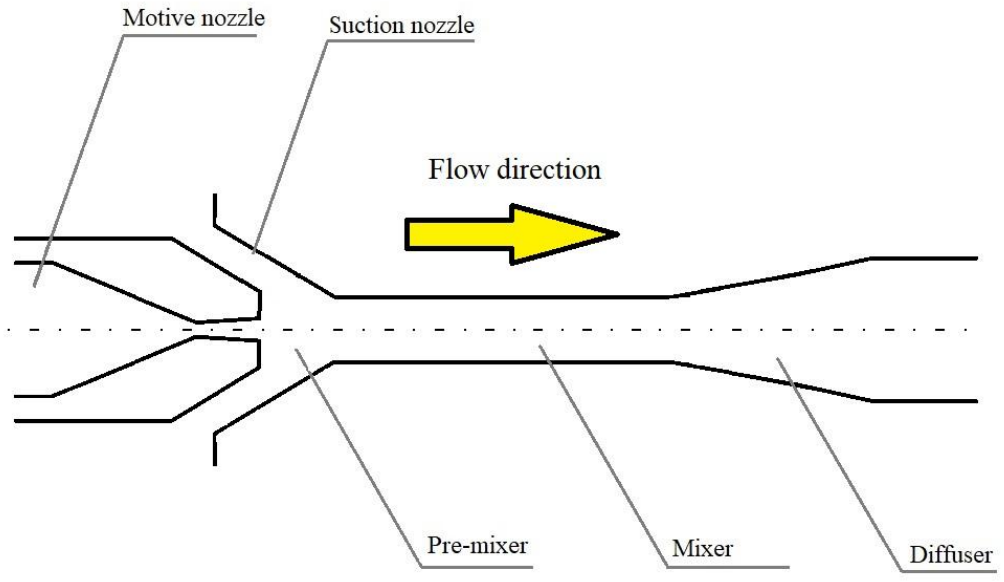

Figure 2 The R744 two-phase ejector geometry.

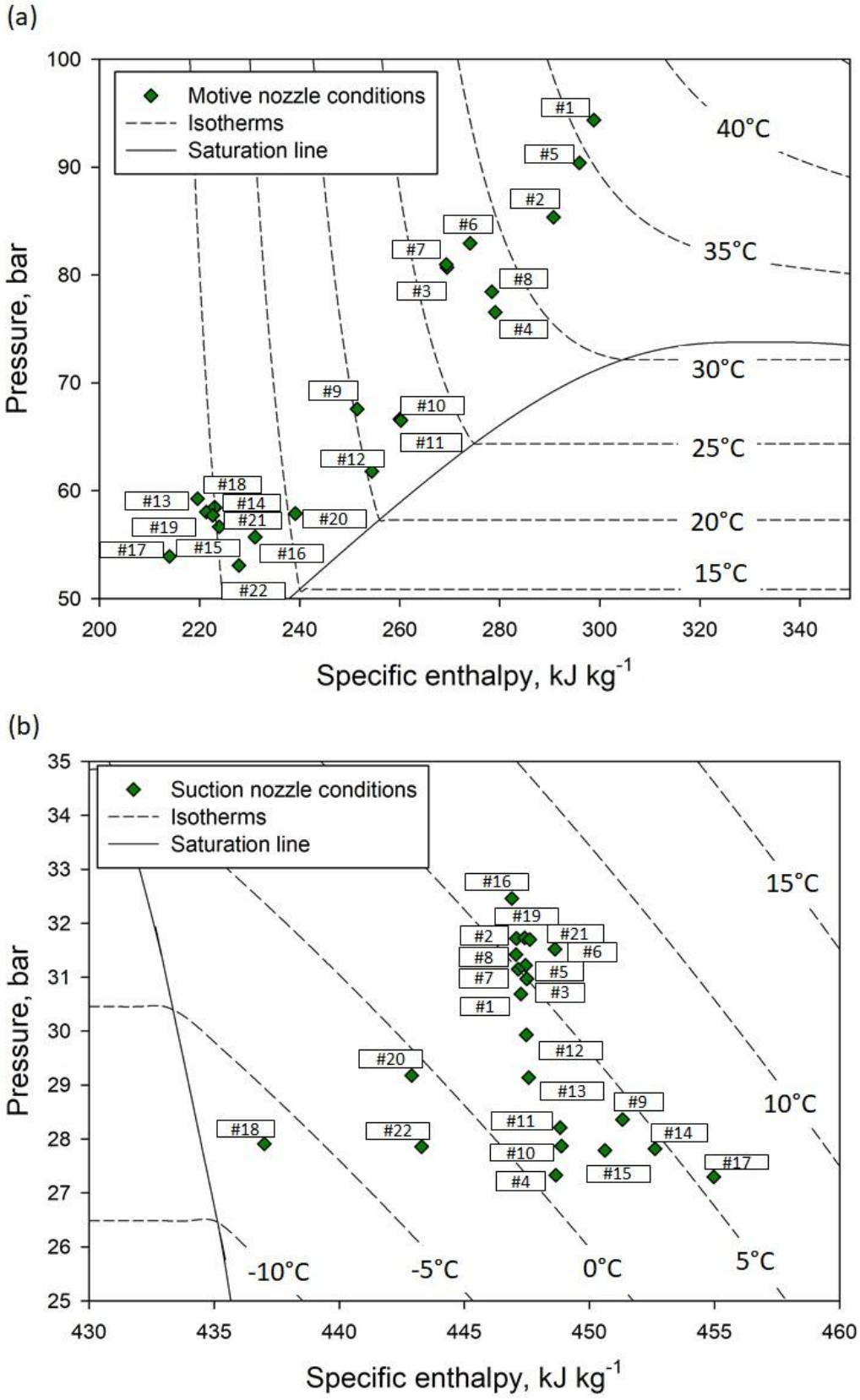

Figure 3 R744 Pressure - specific enthalpy diagram of the operating conditions: (a) motive nozzle and (b) suction nozzle conditions.

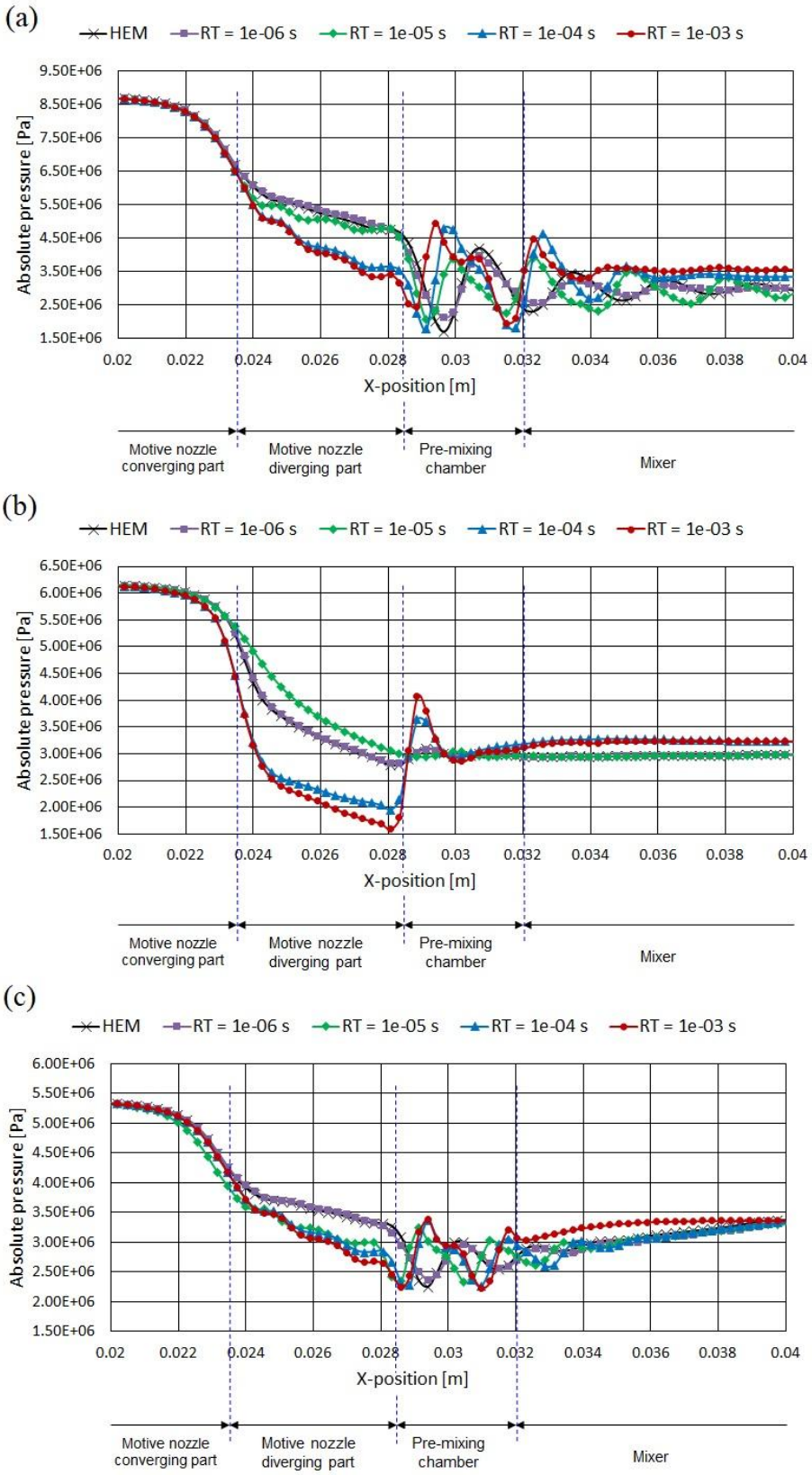

Figure 4 Pressure distribution (in Pa) along axis of the two-phase ejector for HRM with different RT constant θ_0 compared to the HEM results at OC: (a) #2, (b) #12, and (c) #18 presented in Table 2.

(a)

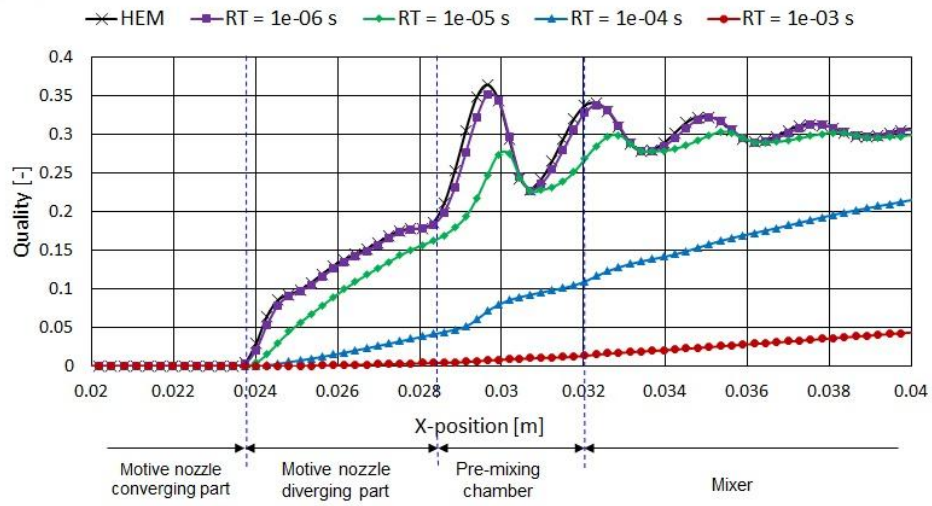

(b)

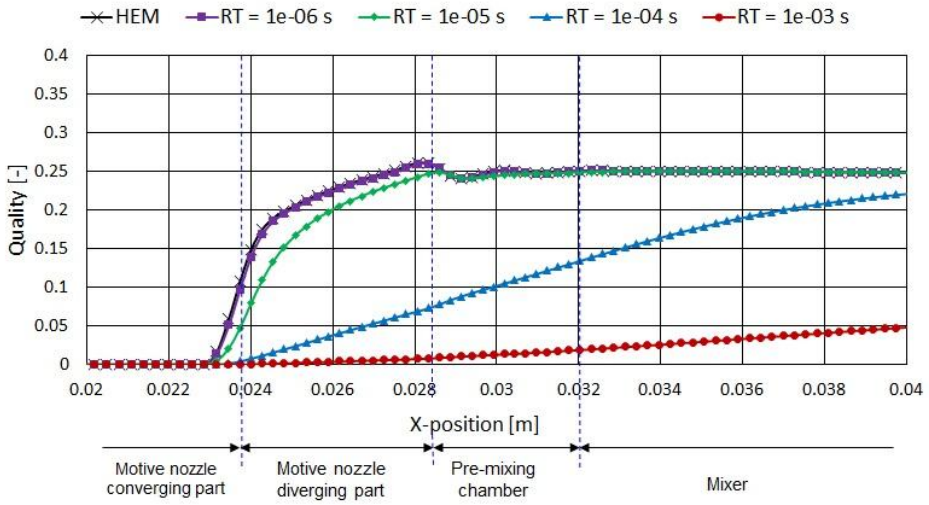

(c)

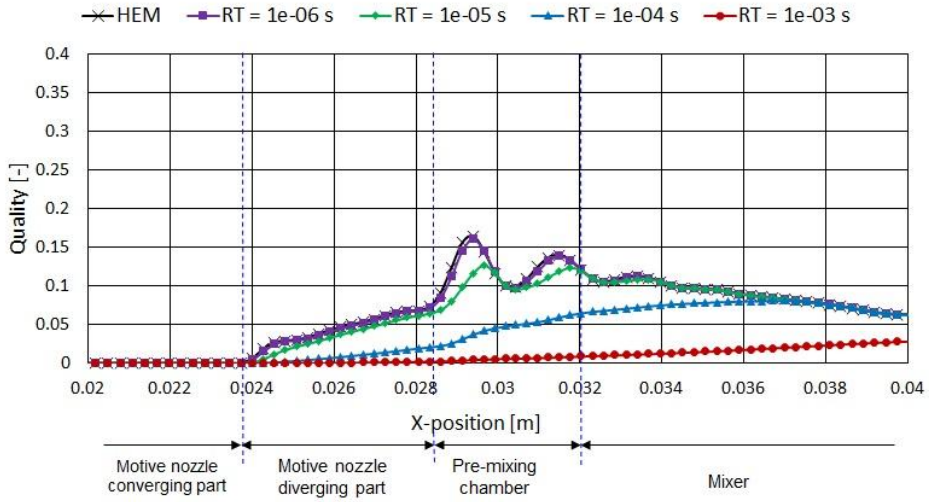

Figure 5 Vapour quality distribution along axis of the two-phase ejector for HRM with different RT constant θ_0 compared to the HEM results at OC #2 (a), #12 (b), and #18 (c) presented in Table 2.

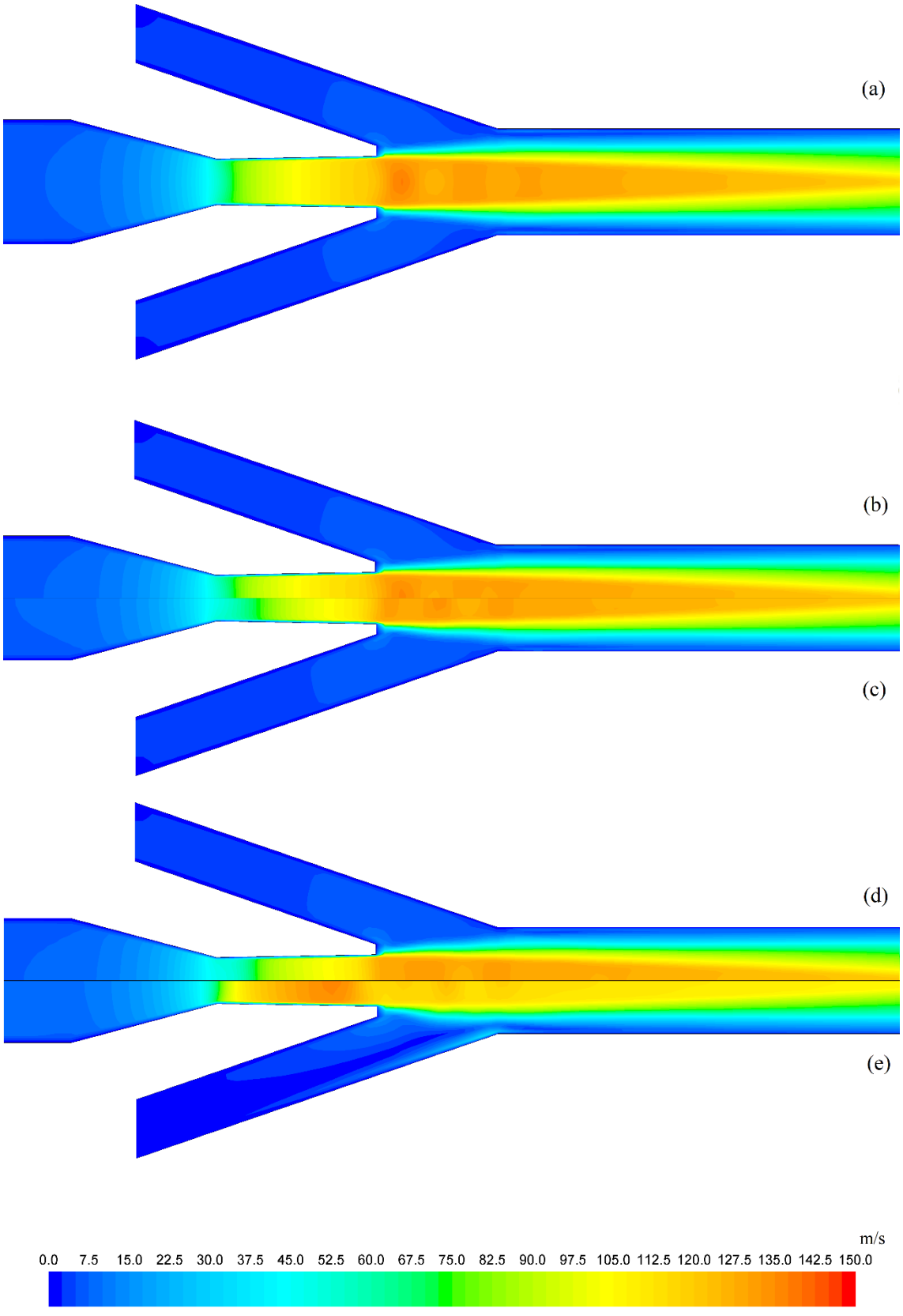

Figure 6 Velocity field (in m/s) for (a) HEM and different RT constants θ_0 of (b) 10^{-6} s, (c) 10^{-5} s, (d) 10^{-4} s, (e) 10^{-3} s for OC #6 presented in Table 2.

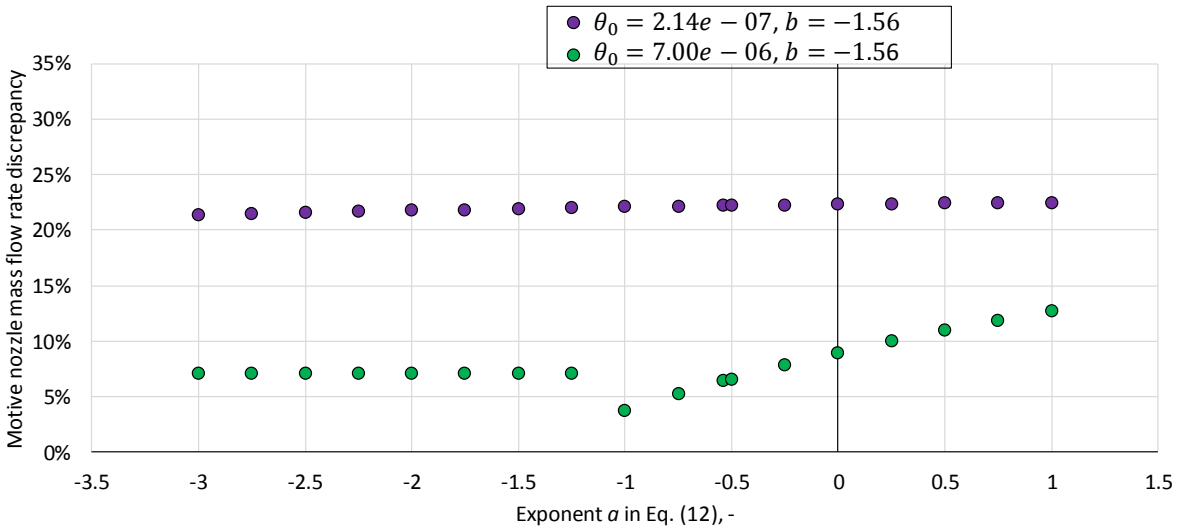

Figure 7 The motive nozzle MFR discrepancy of HRM with different exponent *a* denoted as *a* in Eq. (12) for OC #12 presented in Table 2.

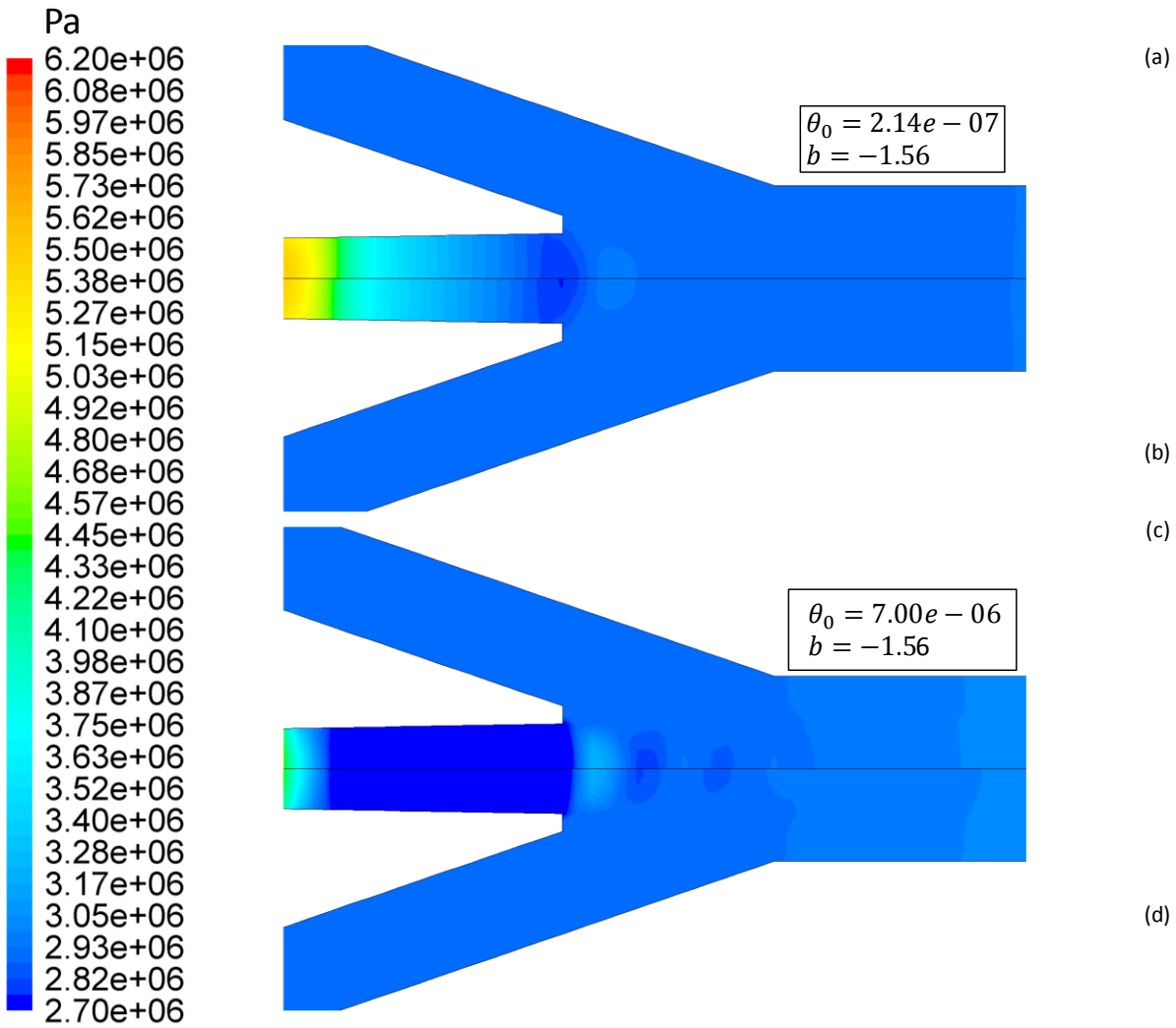

Figure 8 Absolute pressure field (in Pa) for HRM with different constants defined in Eq. (12) for OC #12 presented in Table 2: (a) $a = -1.5$; (b) $a = -1.0$; (c) $a = -1.5$; (d) $a = -1.0$.

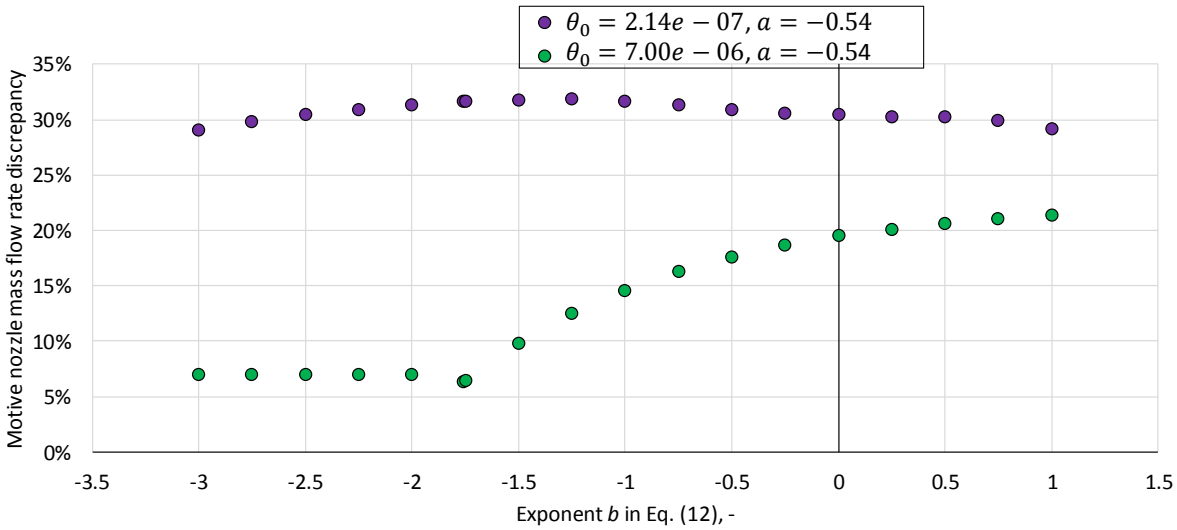

Figure 9 The motive nozzle MFR discrepancy of HRM with different exponent *b* defined in Eq. (12) for OC #12 presented in Table 2.

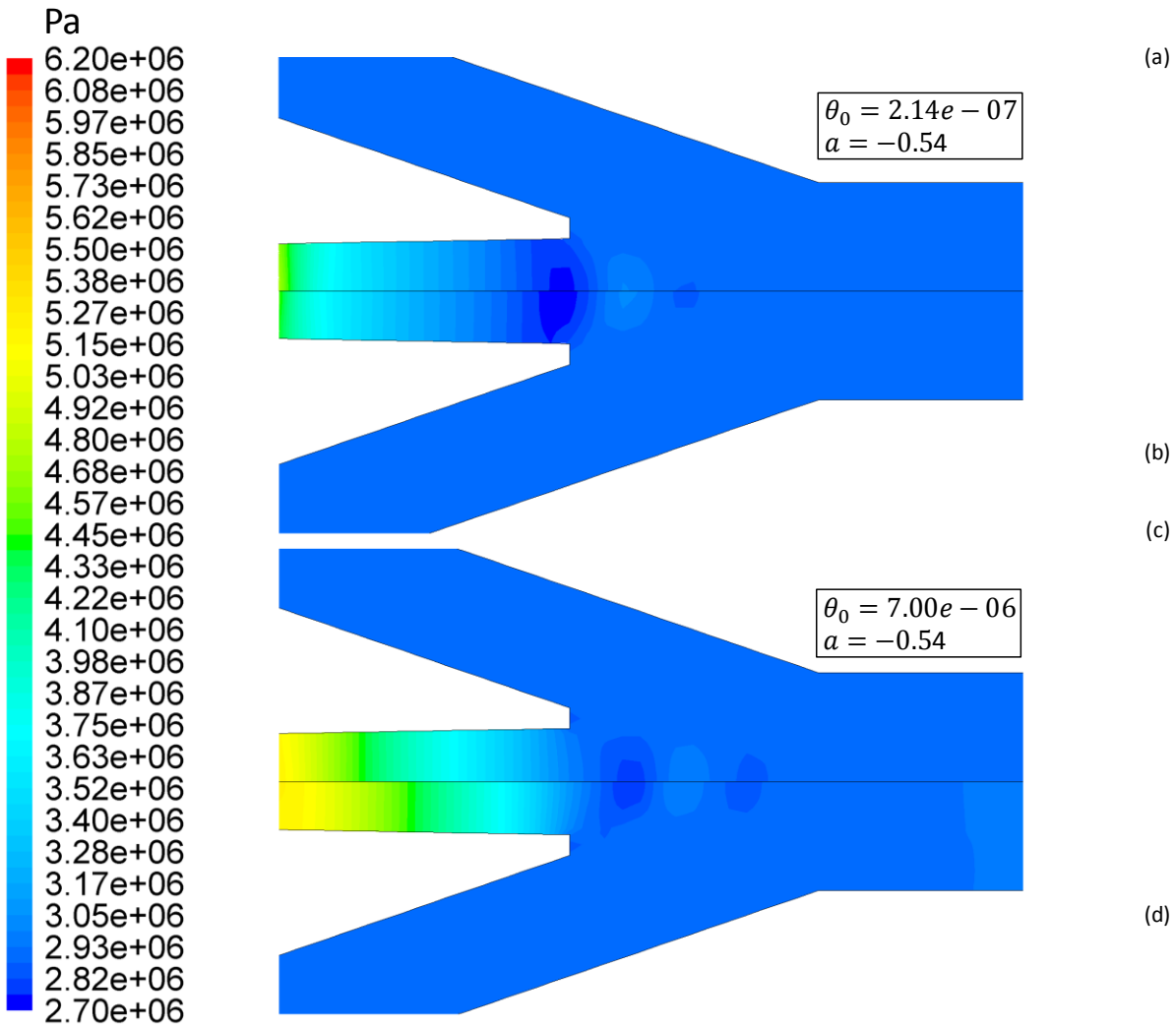

Figure 10 Absolute pressure field (in Pa) for HRM with different constants defined in Eq. (12): (a) $b = -1.5$; (b) $b = -1.0$; (c) $b = -1.5$; (d) $b = -1.0$.

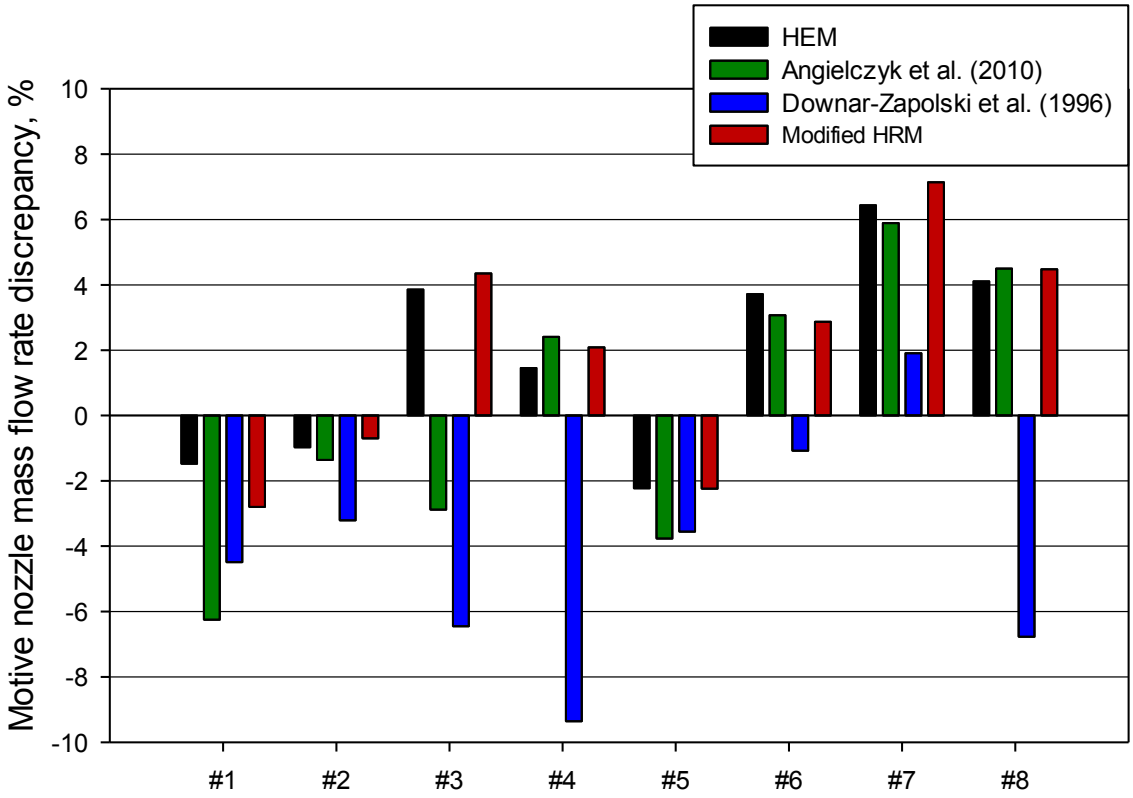

Figure 11 Motive nozzle MFR discrepancy of CFD models at the operating conditions presented in Table 2 for the motive nozzle pressure above the critical point.

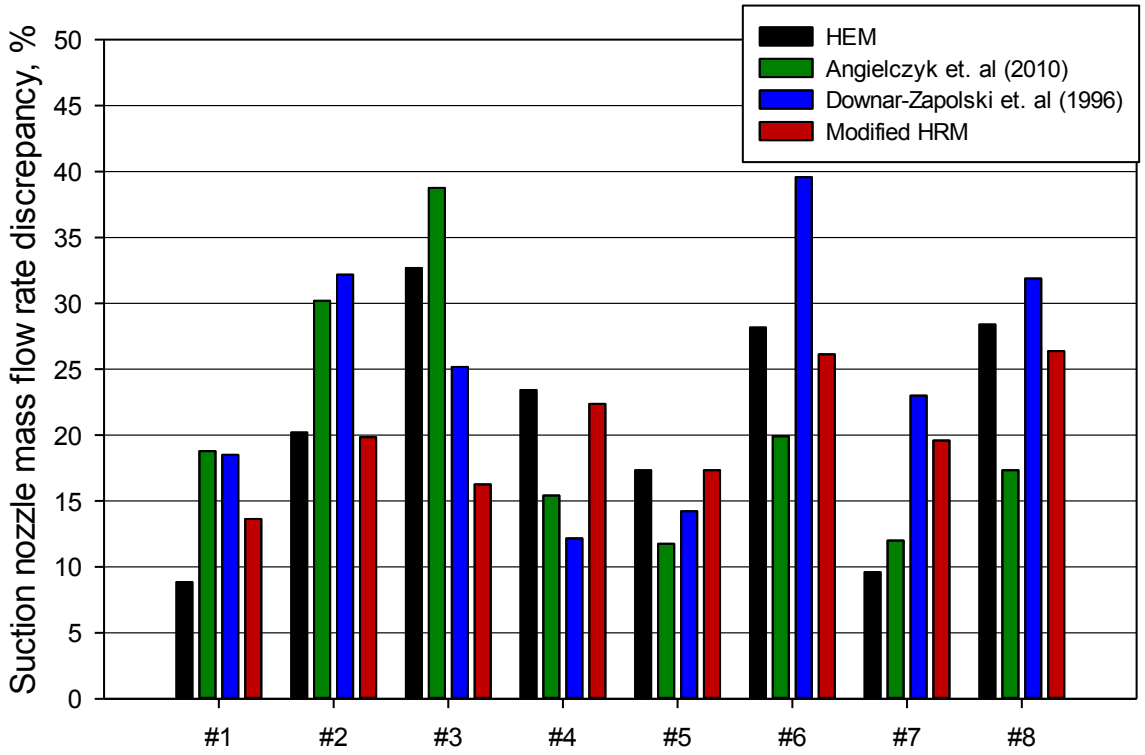

Figure 12 Suction nozzle MFR discrepancy of CFD models at the operating conditions presented in Table 2 for the motive nozzle pressure above the critical point.

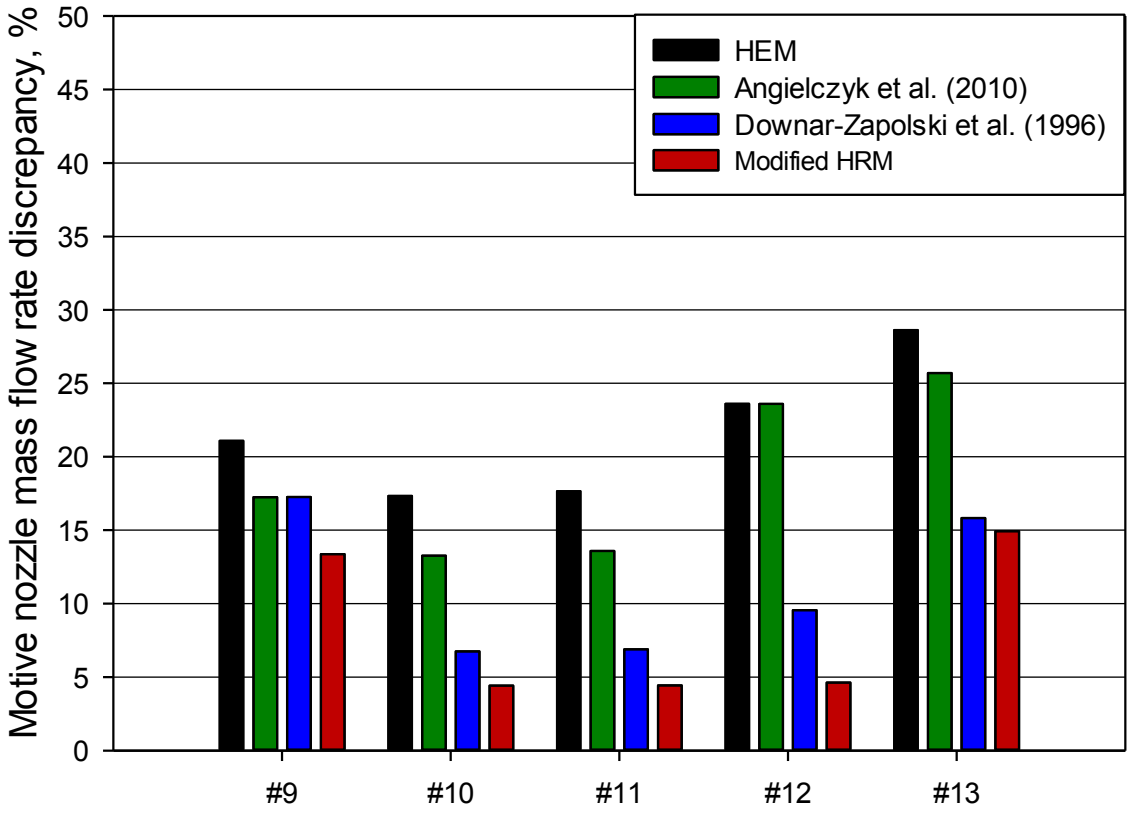

Figure 13 Motive nozzle MFR discrepancy of CFD models at the operating conditions presented in Table 2 for the motive nozzle pressure in the range from 59 bar to the critical point.

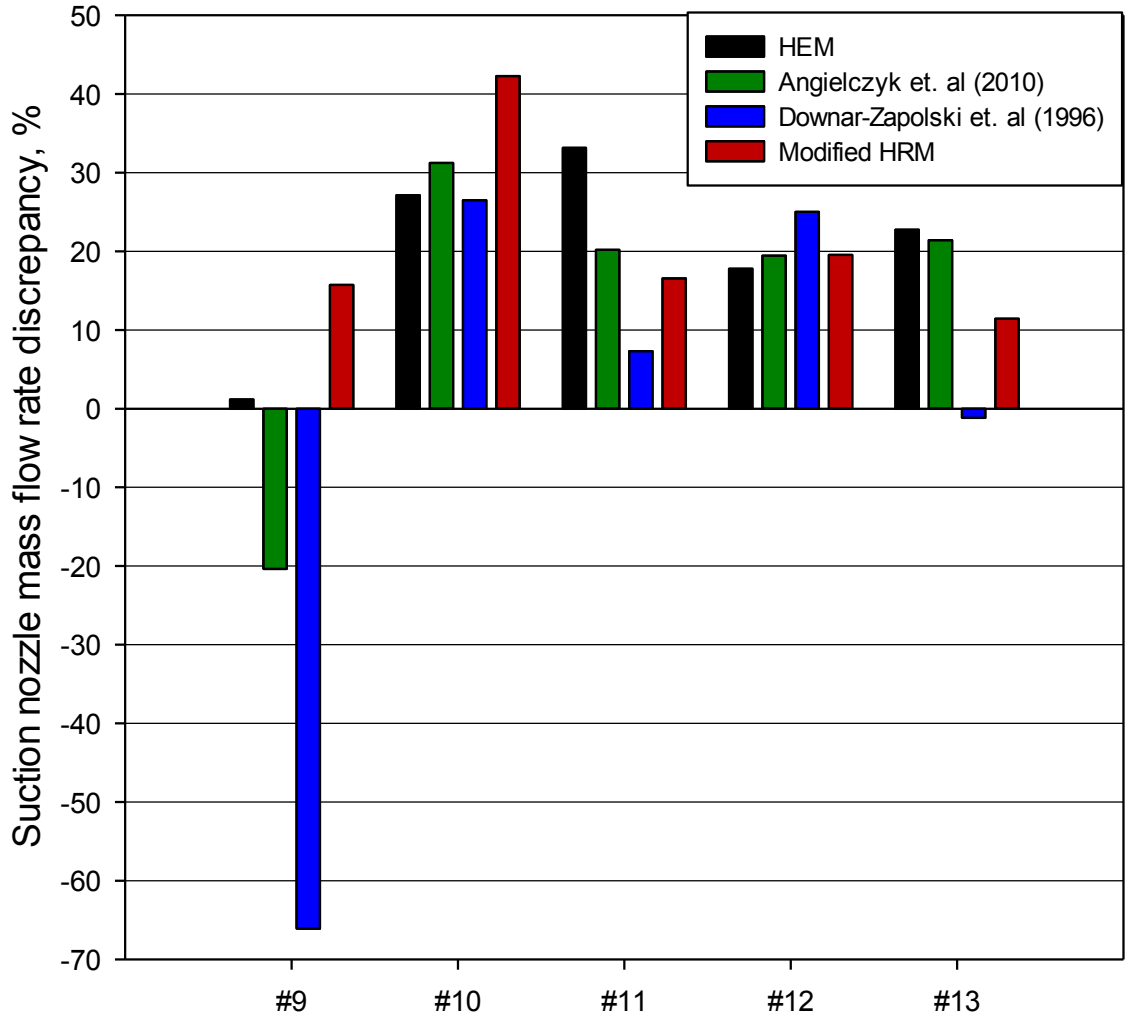

Figure 14 Suction nozzle MFR discrepancy of CFD models at the operating conditions presented in Table 2 for the motive nozzle pressure in the range from 59 bar to the critical point.

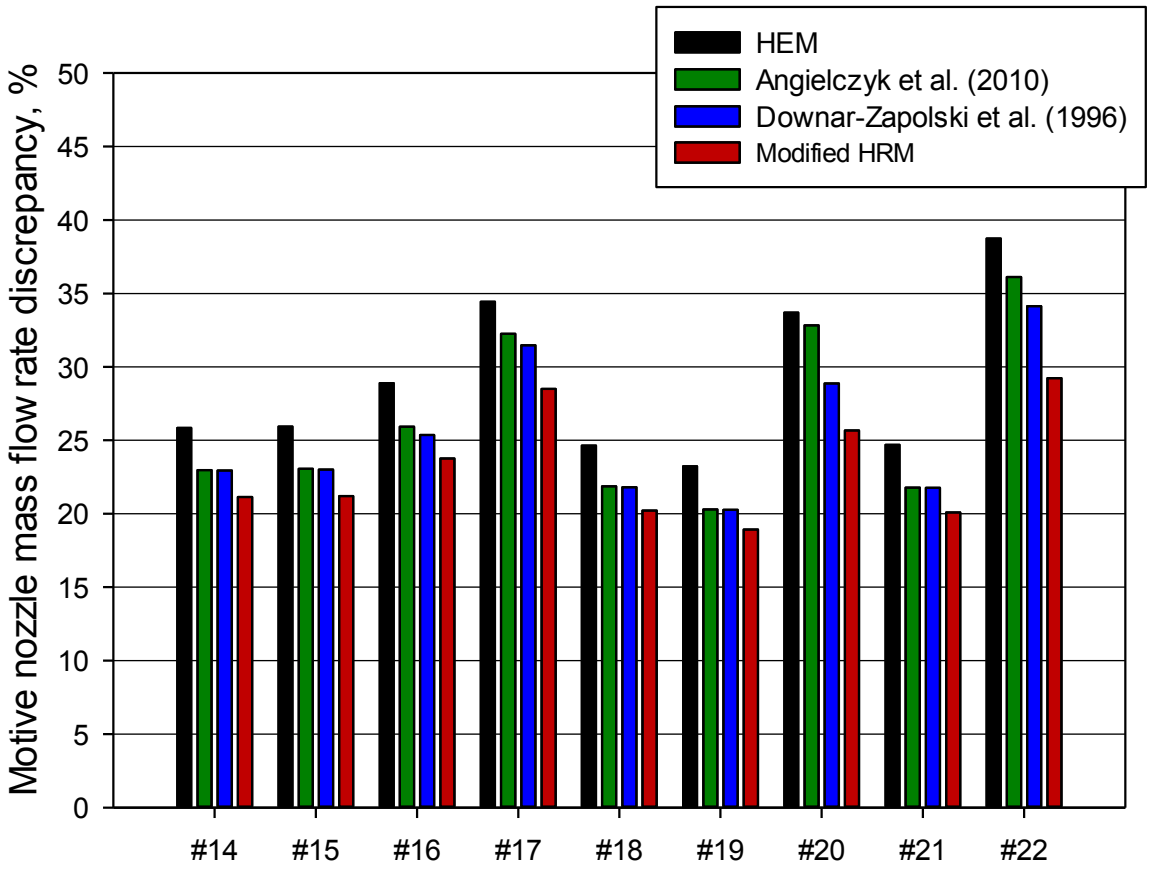

Figure 15 Motive nozzle MFR discrepancy of CFD models at the operating conditions presented in Table 2 for the motive nozzle pressure below 59 bar.

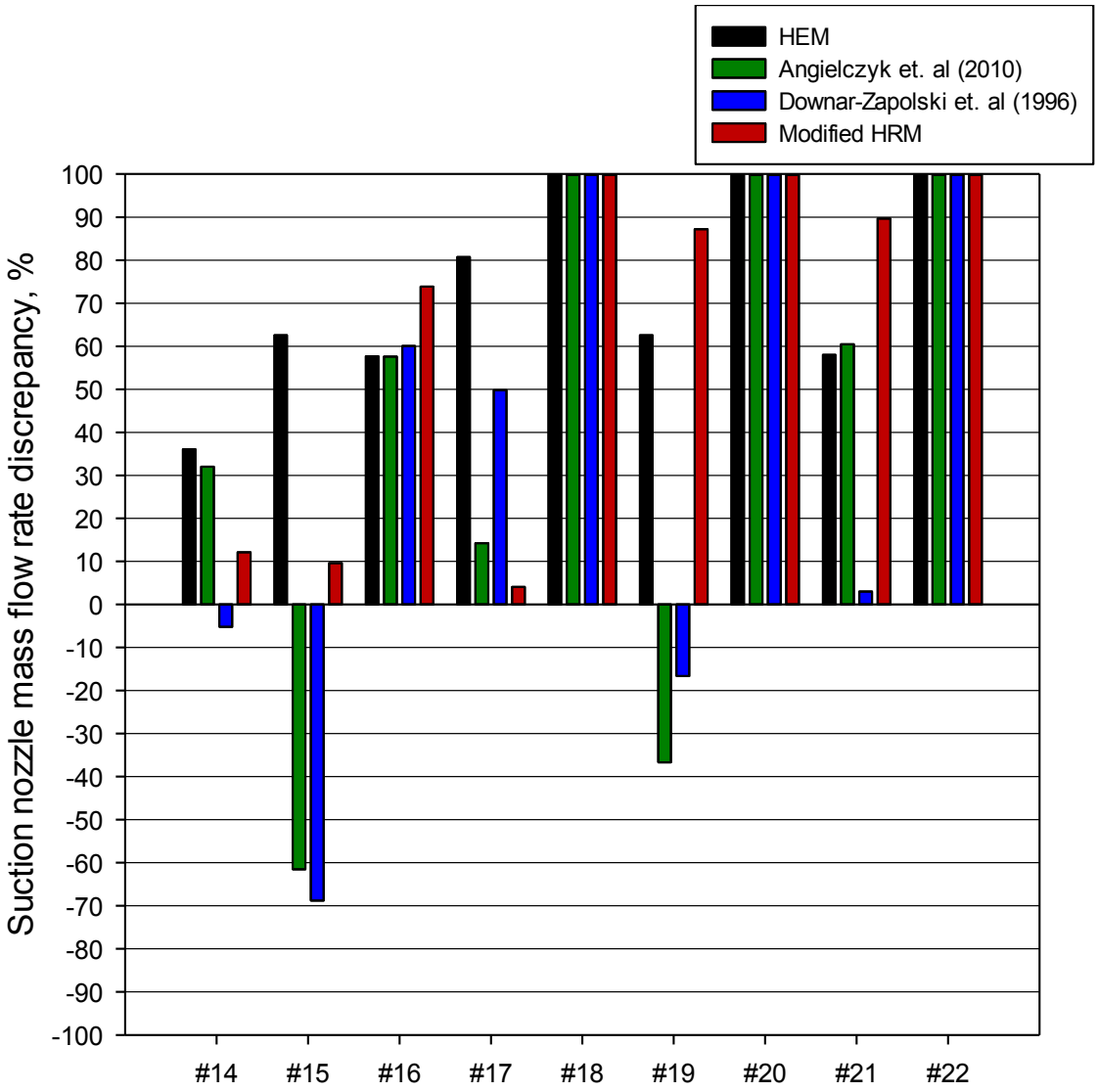

Figure 16 Suction nozzle MFR discrepancy of CFD models at the operating conditions presented in Table 2 for the motive nozzle pressure below 59 bar.

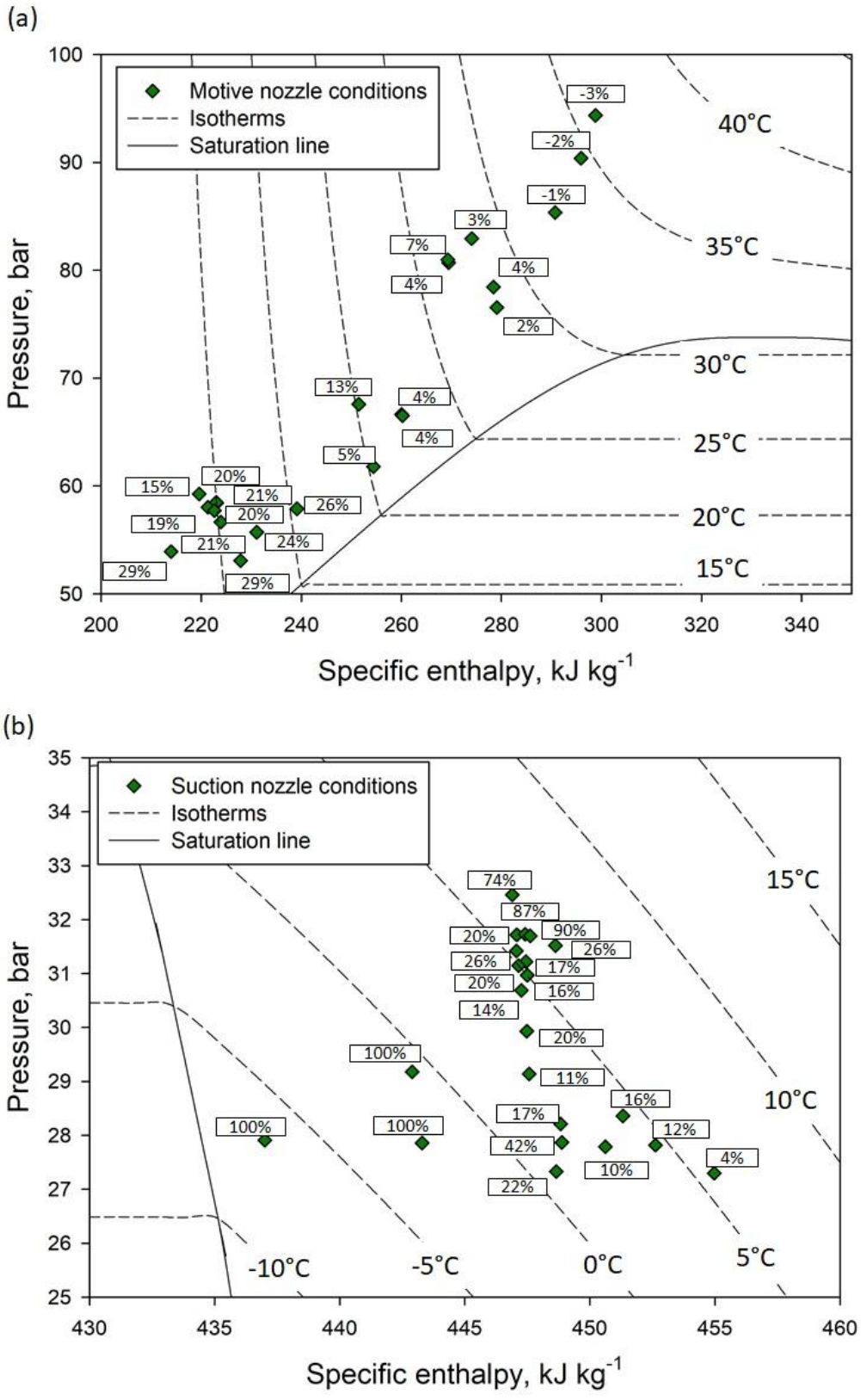

Figure 17 R744 pressure–specific enthalpy diagram of the modified HRM MFR discrepancies at the operating conditions presented in Figure 3 for (a) motive nozzle and (b) suction nozzle.

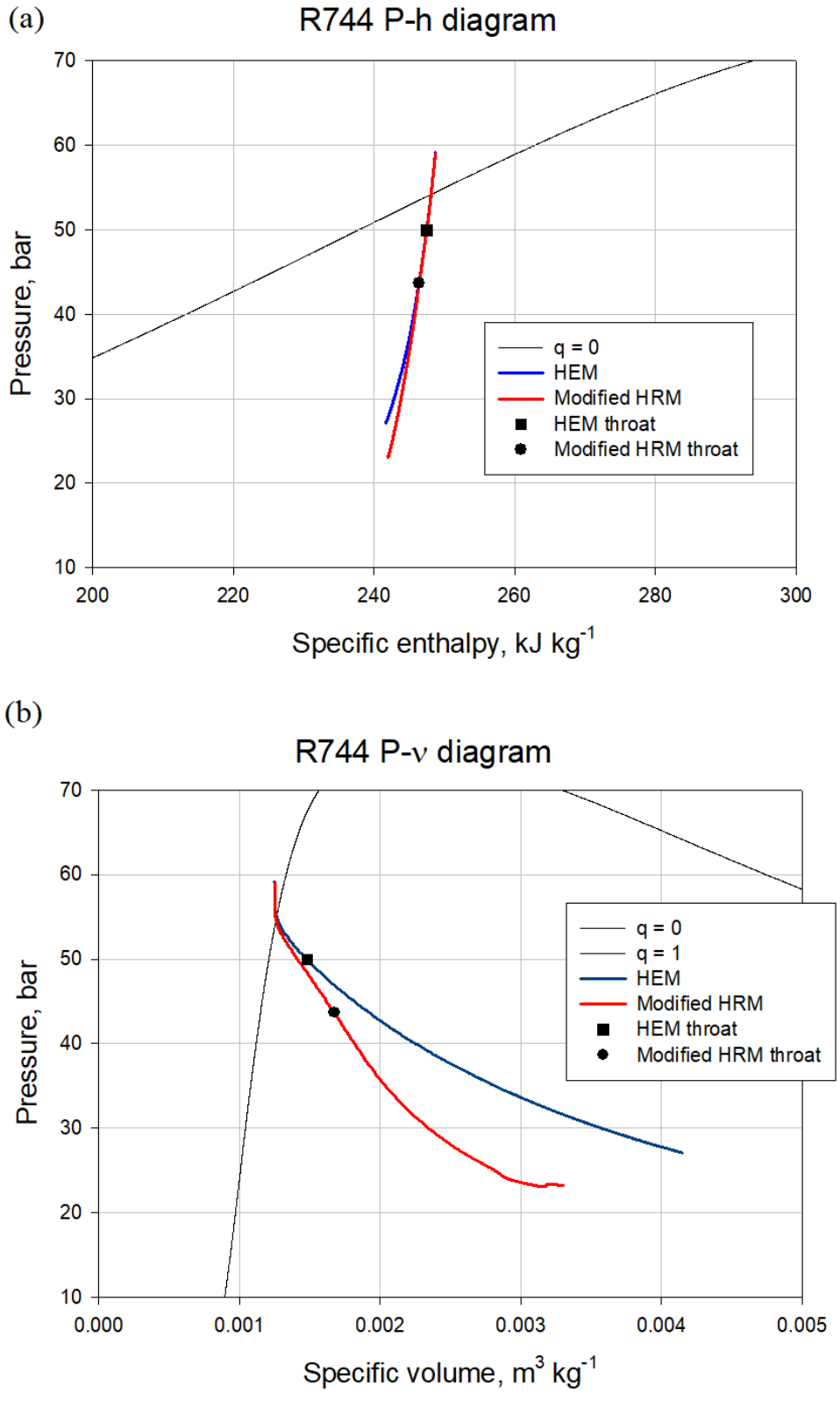

Figure 18 Motive nozzle expansion process for HEM and modified HRM at OC #13 presented in Table 2: (a) pressure-specific enthalpy diagram, (b) pressure-specific volume diagram.

Table 1 The main geometry parameters of the two-phase ejector installed in the multi-ejector module adopted and modified from Banasiak et al. (2015)

Parameters	Geometry
Motive nozzle inlet diameter, 10^{-3} m	3.8
Motive nozzle throat diameter, 10^{-3} m	1.41
Motive nozzle outlet diameter, 10^{-3} m	1.58
Motive nozzle converging angle, °	30
Motive nozzle diverging angle, °	2
Diffuser outlet diameter, 10^{-3} m	8.4
Diffuser angle, °	5

Table 2. Set of the operating conditions (OC) for R744 two-phase ejector.

OC No	Motive nozzle		Suction nozzle		Outlet
	Pressure	Temperature	Pressure	Temperature	Pressure
-	bar	K	bar	K	bar
#1	94.35	309.12	30.69	277.61	35.86
#2	85.35	305.57	31.42	278.45	38.24
#3	80.69	299.97	30.97	278.15	34.39
#4	76.56	301.49	27.33	274.01	32.87
#5	90.39	307.67	31.22	278.45	37.27
#6	82.94	301.48	31.52	279.68	37.32
#7	80.98	299.97	31.15	278.15	34.39
#8	78.45	301.71	31.72	278.86	38.28
#9	67.57	293.33	28.36	277.44	36.77
#10	66.62	295.53	27.87	274.93	32.88
#11	66.51	295.56	28.21	275.36	34.85
#12	61.79	293.42	29.93	276.73	33.87
#13	59.27	281.91	29.14	275.72	34.83
#14	58.41	283.15	27.82	277.71	34.83
#15	56.67	283.35	27.79	276.13	34.87
#16	55.71	285.79	32.46	279.72	36.01
#17	53.93	279.48	27.30	278.85	34.23
#18	58.48	283.14	27.91	266.59	36.80
#19	58.02	282.49	31.73	279.11	36.75
#20	57.89	288.59	29.18	272.45	36.79
#21	57.71	282.94	31.70	279.21	37.17
#22	53.08	284.49	27.86	270.83	34.85

Table 3 Optimised relaxation time coefficients and the minimum objective function OF_{min} for specified motive nozzle pressure ranges.

Motive nozzle pressure range	Operating conditions (see Table 2)	θ_0	a	b	OF_{min}
p_{motive} ≥73.77 bar	#1 ÷ #4	1.00-07	0.00	0.00	2%
59 bar≤ p_{motive} <73.77 bar	#9 ÷ #12	9.00E-06	-0.67	-1.73	6%
p_{motive} < 59 bar	#14 ÷ #17	1.50E-06	-0.67	-2.00	23%